The Pennsylvania State University

The J. Jeffrey and Ann Marie Fox Graduate School

DESIGN AND EVALUATION OF POROSITY IN 3D BONE SCAFFOLD MODELS: COMPUTATIONAL INSIGHTS

A Thesis in

Mechanical Engineering

by

Jonathan Ralph Dsa

Submitted in Partial Fulfillment
of the Requirements
for the Degree of

Master of Science

December 2024

The thesis of Jonathan Ralph Dsa was reviewed and approved by the following:

Sheikh Fahad Ferdous
Assistant Professor of Mechanical Engineering
Thesis Advisor

Anilchandra Attaluri
Associate Professor of School of Science, Engineering and Technology

Ahm E Rahman
Assistant Professor of Mechanical Engineering

Brian Allen Maicke
Associate Professor of Mechanical Engineering
Head of the Department

ABSTRACT

Bones are important organs that provide support, facilitate movement, and protect internal organs. Many conditions, including osteoarthritis, osteomyelitis, osteoporosis, bone defects resulting from trauma and surgery, require the correct selection of bone. Traditional methods such as autologous bone grafting have limitations, which have led to the development of bone healing materials and methods. This study uses CAD-based methods and finite element analysis (FEA) to investigate the design, fabrication, and evaluation of bone scaffolds. Various scaffold designs were developed, and their mechanical properties and porosity were evaluated. This study highlights the importance of improving scaffold design to balance the artificial strength and biological activity required for good bone formation. The results show that the size of the strut can reduce porosity and compressive stress, while a larger area in the scaffold structure increases its resistance to compressive forces. These findings highlight the development of more effective bone repair solutions in orthopedic applications and suggest the development of better bone healing methods.

TABLE OF CONTENTS

LIST OF FIGURES

LIST OF TABLES

ACKNOWLEDGEMENTS

I would like to extend my heartfelt gratitude to all those who have contributed to the successful completion of this project.

Firstly, I would like to thank my advisor, Dr. Sheikh Fahad Ferdous, for his invaluable guidance, continuous support, and insightful feedback throughout the course of this study. His expertise and encouragement have been instrumental in shaping this work.

I am also deeply grateful to the members of my research committee, Dr. Anilchandra Attaluri and Dr. Ahm E Rahman for their constructive criticism and suggestions which have significantly enhanced the quality of this research.

I would like to express my deepest gratitude to my family and friends for their unwavering support, patience, and understanding throughout the duration of my studies. Their encouragement and belief in me have been a constant source of strength.

Thank you all for your invaluable contributions and support.

Chapter 1

Introduction

The human bone is a wonderful organ that is indispensable to human life. It performs several major functions, including giving structural support, enabling movement, and shielding the body's delicate internal organs against impact. Its natural biological importance becomes even clearer with the presence of certain diseases and conditions that afflict it and impair its proper functioning. Three such conditions are osteoarthritis, osteomyelitis, and osteoporosis; they are dangerous not only because they affect the bone but also because they have the potential to seriously undermine the entirety of human health.

In addition to these diseases, traumatic injuries, revision arthroplasties, and tumor resections can result in substantial bone defects or voids. These situations often necessitate bone replacement to restore the affected area's structural integrity and functionality. The need for effective bone replacement solutions is thus critical in managing these conditions and ensuring patients regain their mobility and quality of life. Consequently, developing advanced materials and techniques for bone repair and regeneration is a key focus in orthopedic research and clinical practice.

One current method of bone grafting is autologous bone grafting [1]. This involves taking bone from a healthy area of the patient’s body and transplanting it to the unhealthy area. One of the main advantages of this method is that it uses bone from the body instead of artificial materials, meaning the body can heal itself better. The liver bone is also vascularized, meaning it has blood vessels that feed the bone. This reduces the risk of infection and degeneration from con ditions such as femoral head necrosis. Additionally, the bone graft is removed from the patient's body, so the risk of immune rejection of the implant is lower [2].

The increase in the number of bone disorders or diseases is mainly due to the increase in l ife expectancy of the population, which creates a high demand for bone grafts and bone implants [3]. Large sections of damaged bone must be implanted because they cannot heal themselves, whereas small pieces of damaged bone can heal themselves. Materials with excellent biocompatib ility and mechanical properties should be selected for planting to avoid stress resistance. Stainless steel, titanium and its alloys (Ti-6Al-4V), magnesium-based alloys (Mg-Zn, Mg-Ca,Mg-RE, etc.), Co-Cr-Mo alloys and other metal alloys are frequently used in orthopedic materials. They are used in cultivation due to their healing properties and good biocompatibility [4,5].

The elastic modulus of cortical and trabecular bone varies between 3-30 GPa and 0.02-2 GPa, respectively. Elastic moduli of commonly used metal biomaterials such as stainless steel, Ti-6Al-4V, Co-Cr alloy, and magnesium alloy range from ~210 GPa, ~110 GPa, ~210 GPa, and ~45 GPa respectively [6,7].

Pores were introduced into the implants to prevent elastic modulus mismatched at the bone-implant interfaces. Porosity also aids bone healing by being a source of bone regeneration. While porosity and pore size affect material and biological properties, wall or strut thickness must be optimized to facilitate fabrication.

Greater scaffold porosity increases bone strength, but greater porosity results in less stability. Extensive in vitro and in vivo experiments are required to evaluate the behavior of various scaffold designs, which will cost time and money. Therefore, finite element analysis (FEA) was used to examine the deformation process and stress distribution, thus reducing costs [8].

Rather than trying to reproduce bone structure in bone, many researchers have focused on creating simple models that incorporate tissue repairing strength, density, and porosity, working similarly to those obtained from skin, except for the requirements of material oil. The design concept of porous structure can reduce the strength and stiffness of the scaffold, but the porous structure also provides enough space for new bone to grow. The scaffolding process is based on

computer-aided design (CAD), image-based modelling, implicit surface modeling and topology optimization [9]. CAD-based methods use cylinders, spheres, plates, etc. arranged in rectangular or radial patterns. It provides powerful tools for modeling 3D scaffold geometries such as [10,11]. Most structures are based on regular internal geometries with regular distribution of bacteria.

A simple understanding of how scaffolds can be modified to eliminate the cellular response required for tissue engineering (TE) is important in scaffold engineering and requires a deeper understanding of the effects of the biochemical properties, structure and morphology, biodegradability, and behavior of scaffolds. The main designs of scaffolds for TE applications are shown in Figure 1-1 [12].

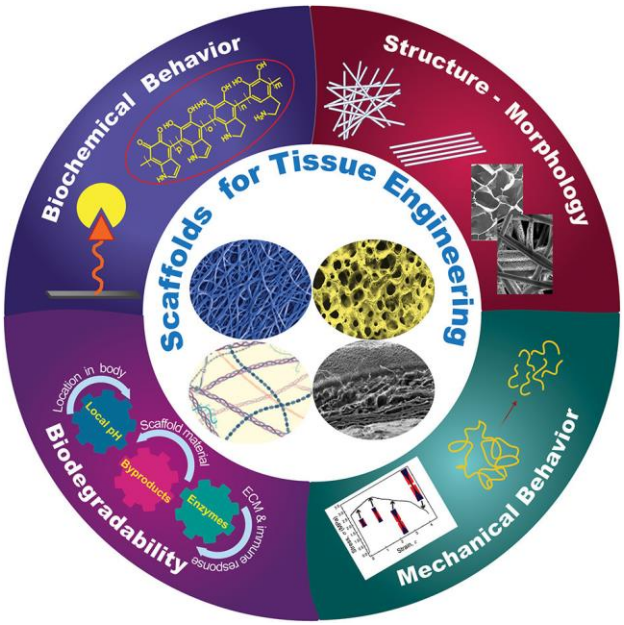

Figure **1-1**: Schematic representation of different design features of biomaterial scaffolds required to elicit the cellular behavior required for tissue applications.

This article compares the compressive strength and porosity of different scaffold designs to find the best scaffold design for bone healing. The goal is to find a scaffold that is strong and porous enough to support cell growth and tissue regeneration while avoiding stress. The study aims to determine the best scaffold design for effective bone healing by evaluating these features.

Chapter 2

Literature Review

Important factors to consider before creating a bone scaffold are biocompatibility, biodegradability, all materials, scaffold structure and production technology. The biocompatibility of the scaffold refers to its ability to support cellular functions (including molecular signals) without affecting the tissue [13,14]. Porosity contributes to the biocompatibility of the scaffold. Bone formation requires a porous structure to accommodate cell growth and transport of nutrients, oxygen, and blood metabolism [15–17].

Conventional manufacturing techniques including electrospinning, particle leaching, freeze-drying, gravity casting, and oil foaming can be used to produce synthetic bone, as shown in Figure 2-1. However, these methods have often been found to be limited in terms of control and pore interconnectivity, which may affect scaffold performance [18].

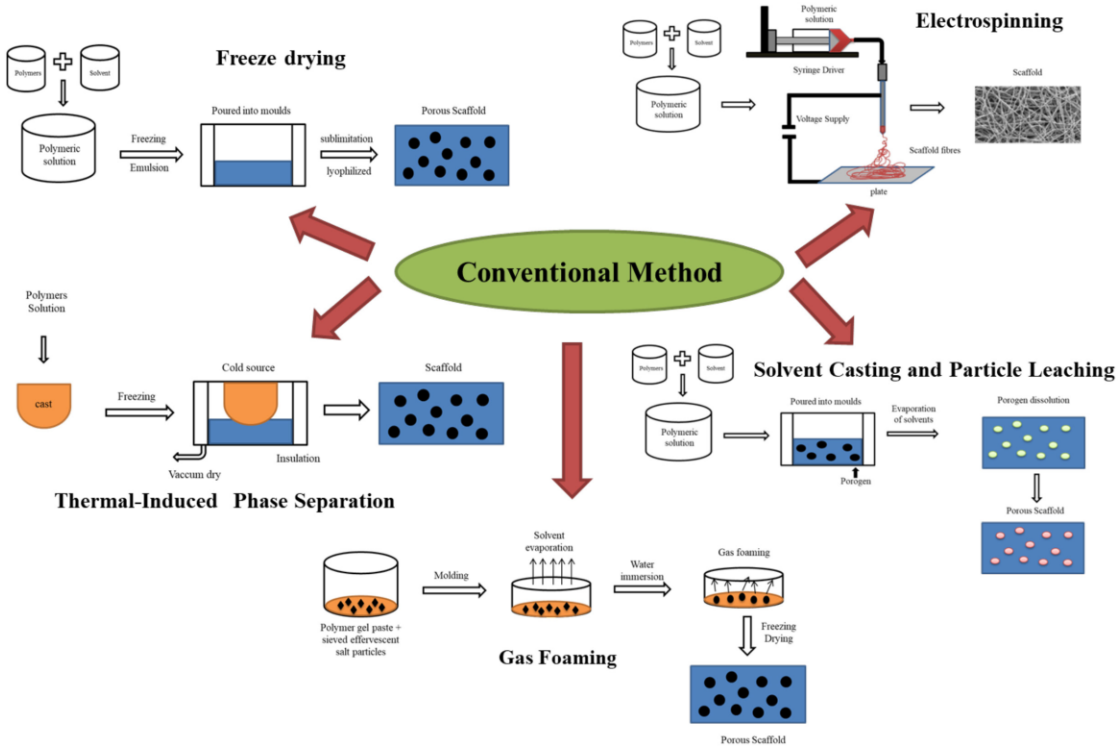

Figure **2-1**: Conventional methods of scaffold fabrication [19].

Porous scaffolds are made using metal-based additive manufacturing (AM) processes such as direct laser deposition, electron beam melting, selective laser melting, and selective laser sintering. Because additive manufacturing techniques can overcome the drawbacks of traditional methods, they are becoming more and more popular in the production of synthetic bone scaffolds. Creating porous scaffolds with graded structures is made possible by the unparalleled flexibility offered by additive manufacturing. By methodically altering strut thickness, pore size, and porosity, this gradation can be obtained [20].

Using a laser energy source to fuse metallic powders layer by layer, selective laser melting (SLM) is a type of powder bed fusion (PBF) AM that fabricates metallic components from CAD data [21] (see Figure 2-2). In order to locally fuse the powder, metallic powder is first applied to each layer, covering the layer before it with a laser beam that is operated selectively. For the

manufacture of metallic lattices, PBF is the recommended technique because direct metal deposition and other alternative metallic AM methods do not offer enough geometric accuracy [22].

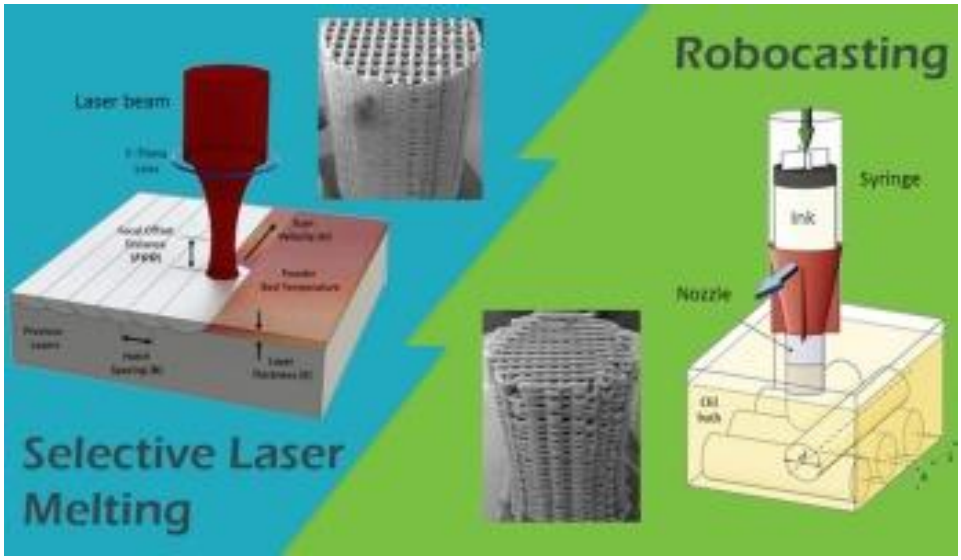

Figure **2-2**: Selective Laser Melting and Robocasting [23].

The size and porosity of the pores also play a significant role in bone ingrowth. Weihu yang et al [24] prepared a porous titanium scaffold with a pore diameter of approximately 650 μm by selective laser melting technology, which had "better bone ingrowth and better bone integration at the bone-scaffold interface than those with pore sizes of 500 and 900 μm". Xijing he et al. [25] prepared a porous titanium scaffold with a pore diameter of 650 μm by selective laser melting technology, which had a "better bone growth effect than those with pore sizes of 400, 500, and 1100 μm". Taniguchi et al. [26] showed that "SLM porous titanium scaffolds with a porosity of approximately 65% and a pore diameter of approximately 600 μm could achieve better stability and bone growth than SLM porous Ti6Al4V implants with pore diameters of 300 μm and 900 μm." In fact, a higher porosity and larger pore size are more favorable for bone ingrowth, although the strength of the scaffold will be compromised [27,28]. As a result, when constructing scaffolds, it is crucial to select scaffolds with a high porosity and pore size to enhance bone growth while maintaining scaffold strength.

Additive manufacturing enables precise control of parameters, promotes appropriate pore connectivity, and promotes appropriate cell ingrowth capacity, creating synthetic bone scaffolds with good mechanical strength and enhanced biospace [29].

With recent advances in additive manufacturing (AM) and new material designs, more and more solutions are entering modern healthcare, including fabric tissue engineering, prosthetics and other biomedical applications. This is mainly due to the possibility of additive manufacturing in creating complex geometries and fixing the material of the structure using various biocompatible materials [30].

A new application of additive manufacturing (AM) in medicine is the production of implants made of lattice-structured materials. These implants play an important role in helping damaged bones heal by stimulating the growth of new bone. Bone scaffolds are widely used to support patients' health by not only reducing pain and increasing disease-related strength and mobility, but also by creating a good place for bone and cell regeneration (see Figure 2-3).

To be effective, bone scaffolds must be carefully designed and constructed to withstand mechanical stress while maintaining a certain level of porosity. This porosity is important because it facilitates cell penetration and growth, thus improving the healing process. Therefore, the production of bone scaffolds has a balance between mechanical strength and porosity to ensure that the scaffold can support the body's function and promote cell growth and bone regeneration.

Although metal additive manufacturing technology provides the opportunity to create models with all possible parameters, not all virtual designs can be transformed into real products [31]. Some of the limitations of this technique include the need for structural support for overhanging struts in the scaffold when the unit cell is large and connected to dust struts. Another problem faced by scaffolds produced by electron beam melting is the removal of sintered powder in the pores of the scaffold [32].

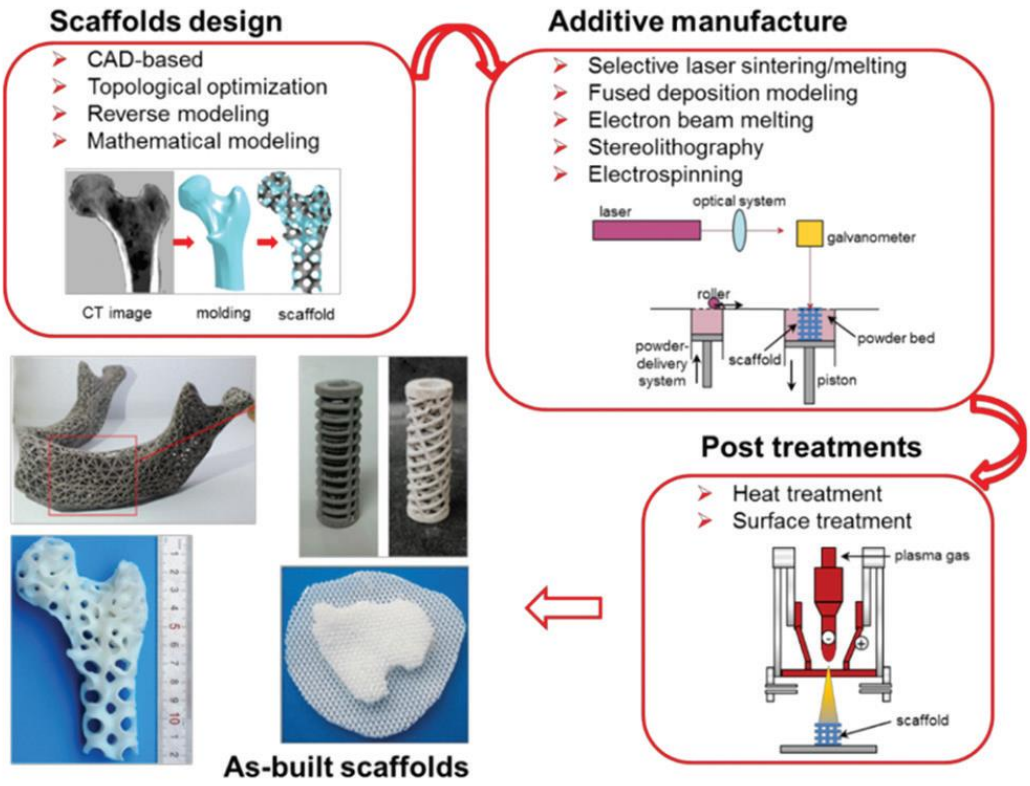

Figure **2-3**: A schematic diagram for the design, additive manufacturing (AM), post-treatments of bone scaffolds, and several typical AM-derived scaffolds [33].

In addition, the creation of 3D biomimetic scaffolds with ordered porous structures often relies on advanced techniques such as computed tomography (CT) and microcomputed tomography (μCT). This imaging technique provides detailed information about the different structures of normal bone and can serve as a template for the creation of scaffolds closer to the entertaining models intended to be replaced. CT and μCT, which capture high-resolution images, can reproduce complex, irregular porosity that is important for cell infiltration and tissue function.

However, the use of this advanced imaging technique has a significant drawback. CT and μCT facilities are expensive and complex, requiring specialized equipment and expertise that may not be easy. In many cases, these ideal sources exceed the actual needs of the stent design, causing unnecessary costs and complications. Therefore, if CT and μCT have differences in reconstructing

bone structure, they need to be carefully evaluated according to all the rules and limitations of the manufacturing process.

A group of materials with artificial engineered structures that are not naturally available in other materials are known as lattice-structured materials. Synthetic microstructures are the main source of the outstanding customized behaviors in lattice materials. The mechanical properties of lattice materials are generated from a repetition of small unit cells in three orientations (see Figure 2-4). These materials can be an excellent solution for bone scaffolding because they are able to provide a variety of mechanical strength, porosity and surface area through different lattice designs which are perfect for promoting osseointegration, bone ingrowth, and implant fixation. Under these conditions, the transport of nutrients and waste is more efficient [34,35].

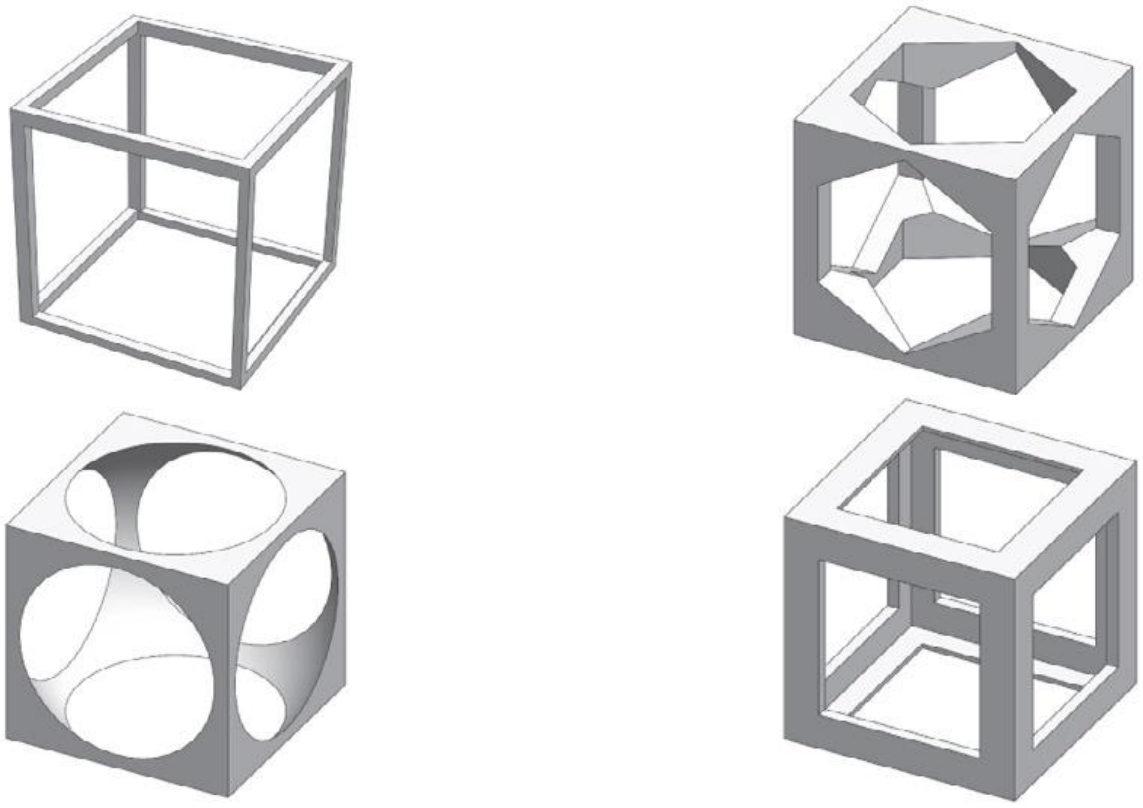

Figure **2-4**: Various unit cells used in designs of scaffolds [21].

Many studies have used finite elements to evaluate the properties of synthetic bone and examine their effects on mechanical properties, transport, and cellular responses. In a study by Smith et al [36], a specific design was “used to compare results calculated from compression test data for polymer-based porous structures created using the design process”. This study concluded that defining the unit cell accurately predicts the overall mechanical behavior of the structure.

Regional Variations in Bone Strength

Shoulder bone

The shoulder bone consists of three parts: the clavicle (collarbone), the scapula (scapula), and the upper arm bone (humerus). The glenoid space, specifically called the glenoid fossa, is part of the shoulder blade. This depression joint serves as a socket for the head of the humerus and forms the ball-and-socket joint of the shoulder called the glenohumeral joint. This joint allows the shoulder to move through a certain range of motion.

According to Frisch et al. [37] they “measured the force distribution of the glenoid bone. The strength of the corresponding subchondral level of the glenoid was on average 66.9 MPa. The higher peaks are measured posteriorly, superiorly and anteriorly with respect to the area of greatest concavity of the glenoid articular surface, known as the bare area. At 1 mm below the subchondral plate the average strength is reduced by 25%, and at 2 mm the strength is reduced by 70%”.

Hip bone

The pelvis, also known as the pubic bone, consists of three parts: the ilium, the ischium, and the pubic bone. The acetabulum is the socket of the hip joint, which houses the head of the femur (thigh bone), forming the ball-and-socket joint of the hip joint. This joint allows for a variety of movements and the carrying of important objects during activities such as walking and running.

Jianyin et al. [38] used "CT scans to measure the biomechanical properties of the hip to create a geometric model of the participants. A 600 N load representing body weight was applied to the sacrum surface to simulate standing on both legs. This study tested three advancements: Group I used an inner plate with a posterior screw, Group II used an outer plate with four corners in the region, and Group III used both sides of the plate. 2.81 mm, while Group I used 2.83 mm. The quadrangular field screw bezel plate (group II) performed similarly to the two bezel plates (group III) and outperformed the rear screw bezel plate (group I)".

Femur

The femur or thigh bone is the longest and strongest bone in the body. It connects from the hip to the knee joint, supports body weight and facilitates movement. The femur is divided into three parts: epiphysis, metaphysis and diaphysis, according to its shape and material density. The bones are cortical bones. It has more bones. The epiphysis and metaphysis are trabecular bones that contain less bone.

From Kumar et al. [39], the model is "CT scanned and then loaded with the participant's body weight. As the load increases, the equilibrium (Von-Mises) voltage increases. The diaphysis has been shown to be the area that can withstand the most stress compared to the rest of the femur".

Conclusion for literature review

Effective bone production requires a balance between biocompatibility, biodegradability, properties and structure. While traditional methods remain insufficient, additive manufacturing (AM), particularly selective laser melting (SLM), provides greater control over scaffold geometry and porosity. The ideal porosity is approximately 600-650 μm, which ensures the growth and stability of bone. Advanced imaging technologies such as CT and μCT can improve the design but are costly. Cage materials are effective and efficient materials and offer practical solutions for the production of durable and functional materials, especially for those with limited resources.

Chapter 3

Materials and Methods

Materials

PLA (Polylactic Acid):

Polylactic acid (PLA) was chosen for its excellent biocompatibility and is approved by the US Food and Drug Administration (FDA) for medical use (Figure 3-1). The Young's modulus of PLA varies between 0.3-4.14 GPa, which is close to the Young's modulus of bone (0.01-2.0 GPa). Young's modulus of 375 MPa, Poisson's ratio of 0.42, and ultimate tensile strength of 15.5 MPa were used in this test. These properties make PLA suitable for bone scaffold development, providing a suitable material while being biodegradable and unlikely to cause any side effects in the body [40].

In this study, PLA will only be used for hollow circular geometries. The many properties of the material make it particularly suitable for implants, providing a good relationship with bone tissue and promoting gradual degradation into new bone, supporting long-term integration and healing.

Figure **3-1**: PLA applications in end-use industries and its' global market consumption [36].

Titanium Alloy Grade 5 (Ti-6Al-4V):

Grade 5 titanium alloy, also known as Ti-6Al-4V, was chosen for its excellent mechanical properties, biocompatibility and corrosion resistance. This alloy is widely used in load-bearing implants as shown in Figure 3-2. Young's modulus of 114 GPa and Poisson's ratio of 0.34 were used in this simulation [41]. Although its higher elastic modulus compared to bone tissue results in increased stress resistance, the use of porous structures in titanium scaffolds helps reduce this by reducing the modulus and promotes stress transfer between the scaffold and bone tissue.

In this study, grade 5 titanium alloy will be used specifically for hollow cubic and truncated hexahedral structures. The porous structure of these structures supports bone tissue integration and long-term physical recovery and reduces stress resistance by taking advantage of the properties of metal.

Figure **3-2**: Applications of titanium alloy in everyday life.

Polycaprolactone-hydroxyapatite(PCL-HA):

Polycaprolactone (PCL) combined with hydroxyapatite (HA) has a promising application for bone scaffold due to its biocompatibility, bioabsorbability, and improved healing properties for composite materials. PCL is known for its flexibility and slow degradation rate; provides all kinds of support during tissue regeneration; It is supported by the osteoconductive properties of HA to promote bone cell attachment and proliferation.

A composite with Young's modulus of 80 MPa, Poisson's ratio of 0.3, and ultimate strength of 15.43 MPa was used in this experiment. However, since there is no data on strength and plastic properties, which are important for modeling and simulation, this mixture will not be used in the simulation.

Simulations Used

Finite element (FE) simulations were used to evaluate the performance of the framework design. The design was made using CAD software (SolidWorks 2023) and was imported into ANSYS 2023 R1 for simulation. Two types of loading were used in the simulation: displacement loading for one layer of the structure and force loading for the other layer. These two methods provide a comprehensive evaluation of the mechanical behaviour of the scaffold. The maximum compressive stress reached by the material is determined by a precise test to ensure the accuracy and reliability of the results.

Design

Modelling Methodology

Several design configurations were created using SolidWorks 2023 comprising three hollow circular units, three hollow cubic units, three truncated hexahedron units [38,39], five hollow hexagonal units, three truncated cube units and one hollow elliptical unit. These designs were then imported to ANSYS to evaluate their structural performance.

Reasons for Choosing Lattice Structures

The choice of lattice structures, including hollow cube, hollow circle, truncated hexahedron, hollow hexagon, truncated cube and hollow elliptical for this thesis is driven by their unique mechanical and biological advantages. These geometries are selected due to their ability to balance mechanical strength and porosity, which are critical factors for bone scaffold performance.

Hollow Cube: This structure offers high mechanical stability and uniform stress distribution, making it suitable for load-bearing applications. Its geometric configuration provides ample surface area for cell attachment and growth while maintaining structural integrity.

Hollow Circle: The circular geometry facilitates better nutrient flow and waste removal, essential for cell viability and proliferation. This structure also mimics natural bone's cylindrical pore shapes, enhancing biocompatibility and integration with host tissue.

Truncated Hexahedron: Known for its high surface-to-volume ratio, this design maximizes the scaffold's porosity without compromising its strength. The truncated hexahedron allows for efficient load transfer and provides a large, interconnected pore network, promoting vascularization and bone ingrowth.

Hollow Hexagon: Characterized by its unique hexagonal shape, this structure combines mechanical strength with enhanced surface properties. The hexagonal geometry offers structural stability and supports uniform cell distribution, facilitating optimal tissue regeneration and integration.

Truncated Cube: Featuring a truncated cubic shape, this scaffold design balances mechanical robustness with porosity. The truncated cube provides a compromise between strength and surface area, crucial for supporting cell attachment and fostering tissue ingrowth in complex bone defects.

Hollow Elliptical: Featuring a hollow elliptical shape, this scaffold design optimizes the balance between mechanical strength and porosity. The elliptical geometry promotes even stress distribution and enhanced load-bearing capacity, crucial for supporting cell attachment and fostering tissue ingrowth in bone tissue engineering applications. This design ensures effective nutrient diffusion and vascularization, mimicking natural bone structure more closely.

These lattice structures were chosen to optimize the scaffolds' mechanical properties and biological functionality, ultimately aiming to develop effective solutions for bone tissue engineering.

Hollow Cube

The structure of the hollow cubic unit cell is the length of the frame *l* and the thickness t. In this design, the strut length of each element is fixed as l = 3 mm, while the strut thickness varies according to the values t = 0.25 mm, t = 0.5 mm and t = 1 mm as illustrated in Table 3-1.

Truncated Hexahedron (THH)

The strut length *l* of each octagon was kept constant at 1 mm, while the strut thickness t was varied between 0.25 mm, 0.5 mm, and 1 mm to produce different THH unit cells as illustrated in Table 3-1.

Table **3-1**: Designs of the hollow cube and truncated hexahedron units and their scaffolds [41].

Unit cell	Scaffold	Specification
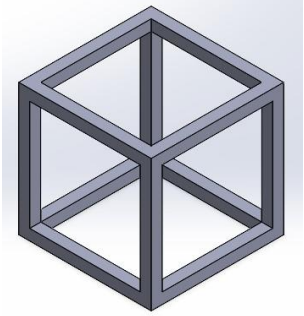 Hollow Cube 1	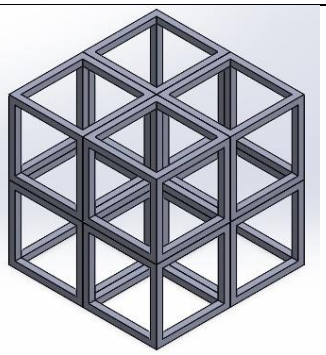	Thickness of strut (0.25×0.25 mm^2) Porosity (95%)

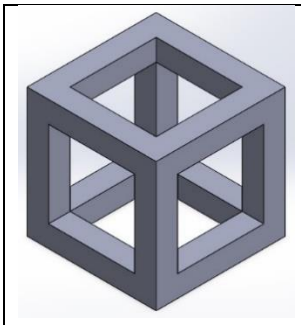 Hollow Cube 2	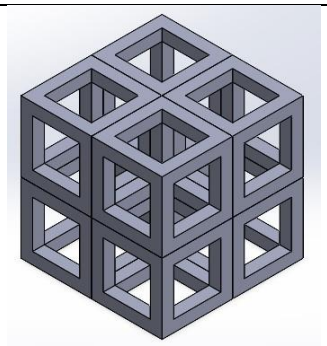	Thickness of strut (0.5×0.5 mm^2) Porosity (82%)
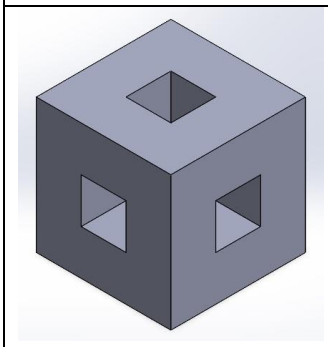 Hollow Cube 3	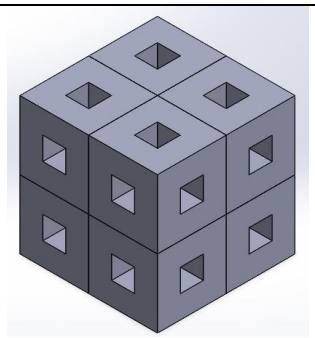	Thickness of strut (1×1 mm^2) Porosity (62%)
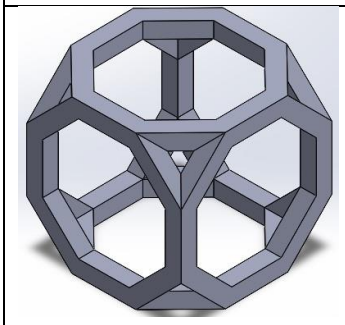 THH 1	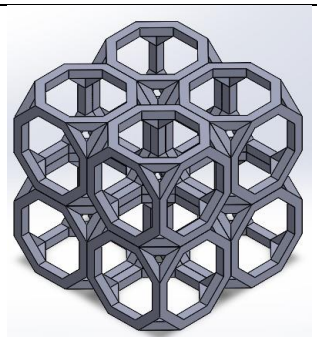	Thickness of strut (0.25×0.25 mm^2) Porosity (91%)

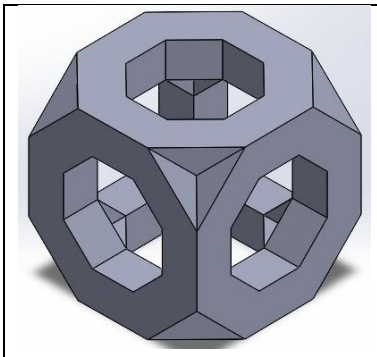 THH 2	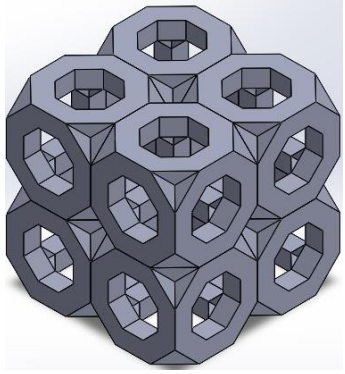	Thickness of strut (0.5×0.5 mm^2) Porosity (70%)
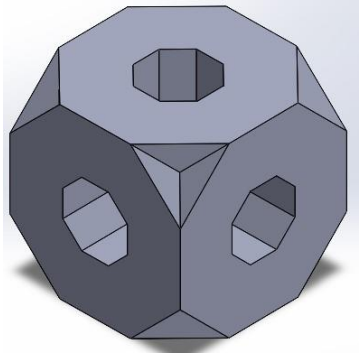 THH 3	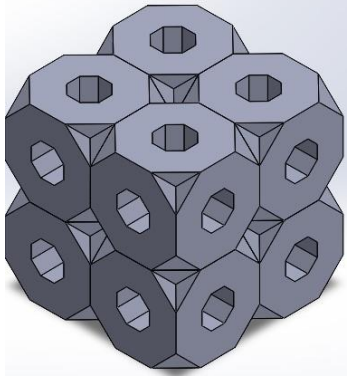	Thickness of strut (1×1 mm^2) Porosity (22%)

Hollow Circle

The overall size of the hollow circular geometry is 12 mm × 12 mm × 12 mm. In this framework, the pore sizes vary in number and size to adapt to different designs. Despite the changes in the number of cells, the porosity and pore volume remain at a constant level to ensure consistency in materials and geometric shapes.

Table **3-2**: Various hollow circle cell sizes and their geometries [40].

No.	Parameter	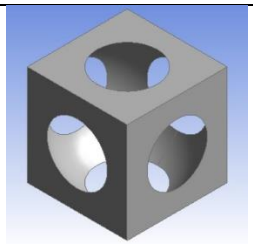	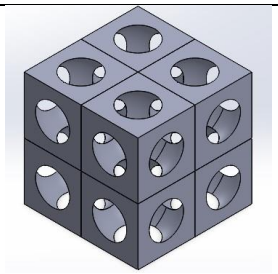	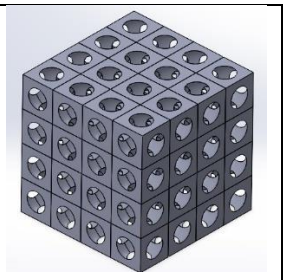
1	Model name	C1	C8	C64
2	Cell size (mm)	L=12, d=10	L=6, d=5	L=3, d=2.5
3	No. of cells in each direction	1	2	4
4	Porosity	81%	81%	81%
5	Surface Area (mm^2)	675.22	957.67	1522.57

L= length of the unit cell; d= diameter of the pore

Hollow Hexagon

The hollow hexagonal structure consists of hexagonal cells arranged in a 2x2 matrix. The hexagonal cells vary in size to accommodate different design parameters. The variation in cell size

allows for adjustments in porosity and porous volume across the scaffold, tailored to specific structural requirements.

Table **3**-**3**: Various designs of the hollow hexagonal scaffolds

Scaffold	Model name	Specifications
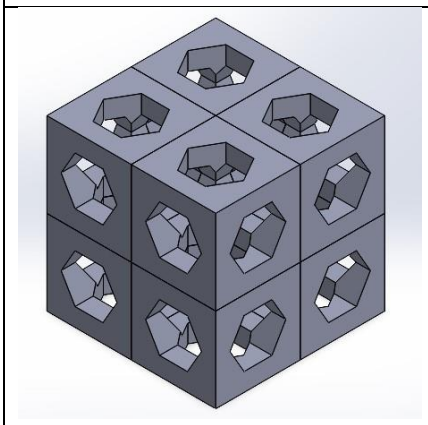	Hollow Hexagon 1 (HH1)	Cell size: 5x5x5 mm^3 Pore dimensions: 1.65 mm Porosity: 50%
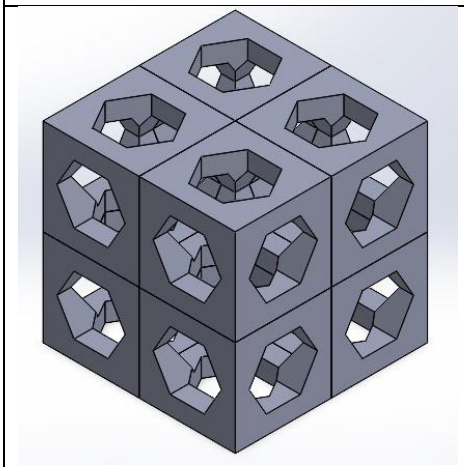	Hollow Hexagon 2 (HH2)	Cell size: 5x5x5 mm^3 Pore dimensions: 1.77 mm Porosity: 60%

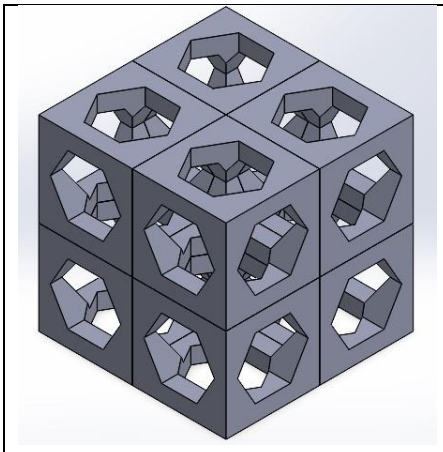	Hollow Hexagon 3 (HH3)	Cell size: 5x5x5 mm^3 Pore dimensions: 1.88 mm Porosity: 70%
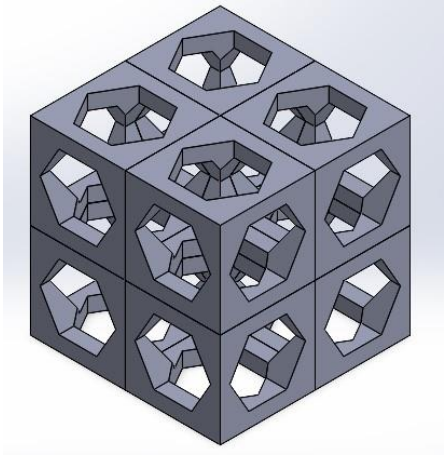	Hollow Hexagon 4 (HH4)	Cell size: 5x5x5 mm^3 Pore dimensions: 1.99 mm Porosity: 80%
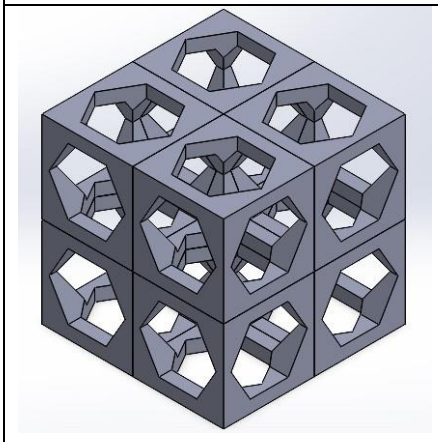	Hollow Hexagon 5 (HH5)	Cell size: 5x5x5 mm^3 Pore dimensions: 2.09 mm Porosity: 90%

Truncated Cube

The truncated cube structure has a 2x2 matrix, within the 5mm x 5mm x 5mm x 5mm framework. These cells are varied in size to explore different geometric configurations while adjusting porosity and porous volume throughout the scaffold. Flexibility in meeting diverse structural demands is ensured by this design approach.

Table **3**-**4**: Various designs of the truncated cube scaffolds

Scaffold	Model name	Specifications
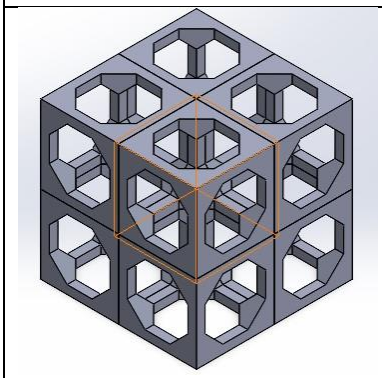	Truncated Cube 1 (TRC1)	Cell size: 5x5x5 mm^3 Pore dimensions: 1.61 mm Porosity: 50%
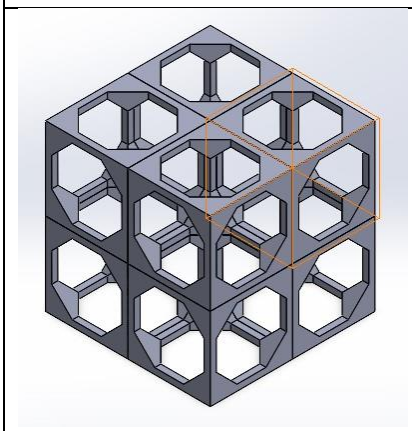	Truncated Cube 2 (TRC2)	Cell size: 5x5x5 mm^3 Pore dimensions: 1.76 mm Porosity: 60%

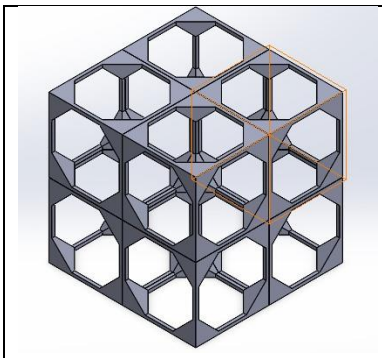	Truncated Cube 3 (TRC3)	Cell size: 5x5x5 mm^3 Pore dimensions: 1.90 mm Porosity: 70%

Hollow Elliptical

The hollow elliptical structure contains elliptical cells integrated into a 2x2 matrix in a 5 mm outer box on each side. This scaffold uses two types of units to achieve different porosity: one layer (large elliptical unit cell) with 4.5 mm long axis and 2.5 mm short axis and one with 3.5 mm long axis and 1.5 mm minor axis another layer (small elliptical unit cell). The design explores different geometric configurations by adjusting the porosity and pore volume of the entire scaffold. For detailed dimensions of the unit cells, refer to Table 3-5. The use of different porosities makes it easier to meet different design requirements and enhances the performance of the scaffold to improve overall properties and biointegration.

Table **3-5**: Table of unit cell dimensions for hollow elliptical scaffold

No.	Parameter	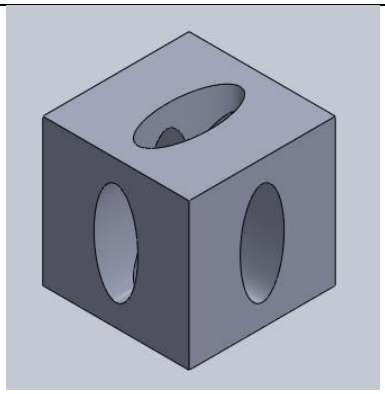	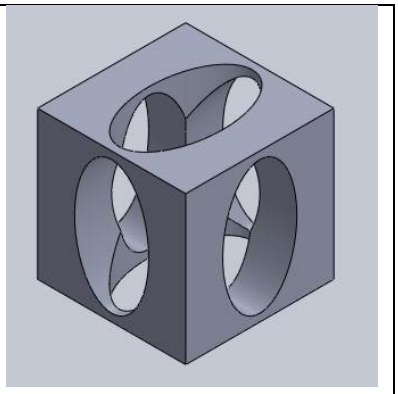
1.	Model name	Smaller elliptical unit cell	Larger elliptical unit cell
2.	Cell size	Major axis: 3.5 mm Minor axis: 1.5 mm	Major axis: 4.5 mm Minor axis: 2.5 mm
3.	Porosity	16	35
4.	Surface Area (mm^2)	261.53	330.64

This scaffold features a 2x2 matrix of unit cells, with varying porosity, as shown in Figure 3-3 below. The anterior and frontal parts have large elliptical unit cells (4.5 mm major axis and 2.5 mm minor axis), while the lower posterior and frontal parts have small elliptical unit cells (3.5 mm major axis and 1.5 mm minor axis).

Both mechanical strength and biological function can be enhanced by the alternating arrangement of larger and smaller unit cells. Structural integrity is ensured by the smaller unit cells.

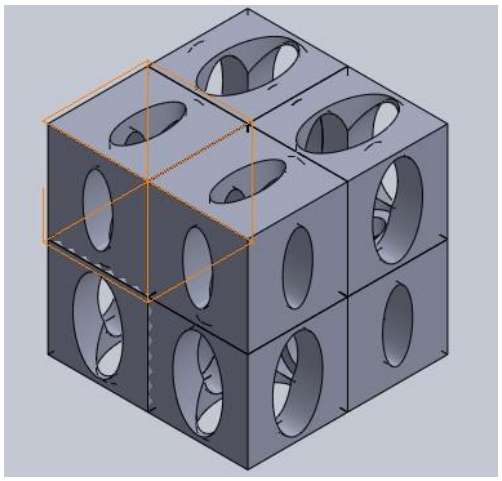

Figure **3-3**: Schematic of the hollow elliptical scaffold. The 2x2 matrix shows larger elliptical unit cells at the bottom front and top back, and smaller elliptical unit cells at the bottom back and top front.

Governing Equations

The structural equations used in this study ensure that the simulated structure remains in static equilibrium under loads and constraints. These equations are important to verify the accuracy and reliability of finite element analysis (FEA) results. They are shown as follows:

1. Force Equilibrium:

   $\sum F_x=0,$

   $\sum F_y=0,$ (Equation 1)

   $\sum Fz=0$

   These equations indicate that the sum of forces in the x, y, and z directions must be zero, ensuring translational equilibrium.

2. Moment Equilibrium:

   $\sum \vec{M_O}=0$ (Equation 2)

This equation dictates that the sum of moments around a reference point O must be zero, ensuring rotational equilibrium.

3. The finite element analysis (FEA) in this study is governed by the basic equations of linear elasticity, given by:

$$\sigma = E\,\varepsilon \qquad \text{(Equation 3)}$$

where σ is the stress, E is the Young's modulus, and ε is the strain.

4. The porosity is calculated using the following equation:

$$\text{Porosity} = (\text{Porous Volume}/\ \text{Total Volume}) \times 100\% \qquad \text{(Equation 4)}$$

5. For the nonlinear analysis, to determine the approximate plastic strain and stress, the Ramberg Osgood equation was used to determine the values:

$$\sigma = K \cdot \varepsilon + (E/\sigma_y) \cdot (\varepsilon)^n \qquad \text{(Equation 5)}$$

Where:

- σ is the stress,
- ε is the strain,
- K is the elastic modulus of the material,
- σ_y is the yield stress,
- E is the Young's modulus of the material,
- n is the strain-hardening exponent.

This equation helps to model the stress-strain relationship beyond the linear elastic region, considering both the elastic and plastic deformation behaviours of the material [42].

Surface Area

Surface area is important in scaffold design because more surface area can improve bone formation. In this study, the surface area of the assembled unit was calculated using SolidWorks' quality measurement tool. The results show that the surface area increases with the thickness and geometric dimensions of the model.

Mesh Sensitivity Analysis

Grid independence tests are performed to ensure that the simulation process has sufficient detail to complete the numerical tests. This involves running the simulation multiple times while gradually increasing the content until the results are stable. To achieve good results, each model is meshed using quadratic elements with different mesh sizes. This iterative process helps to accurately and reliably determine the correct mesh size, as illustrated in Figure 3-4 which presents the mesh sensitivity analysis of a Hollow Hexagon model (HH2).

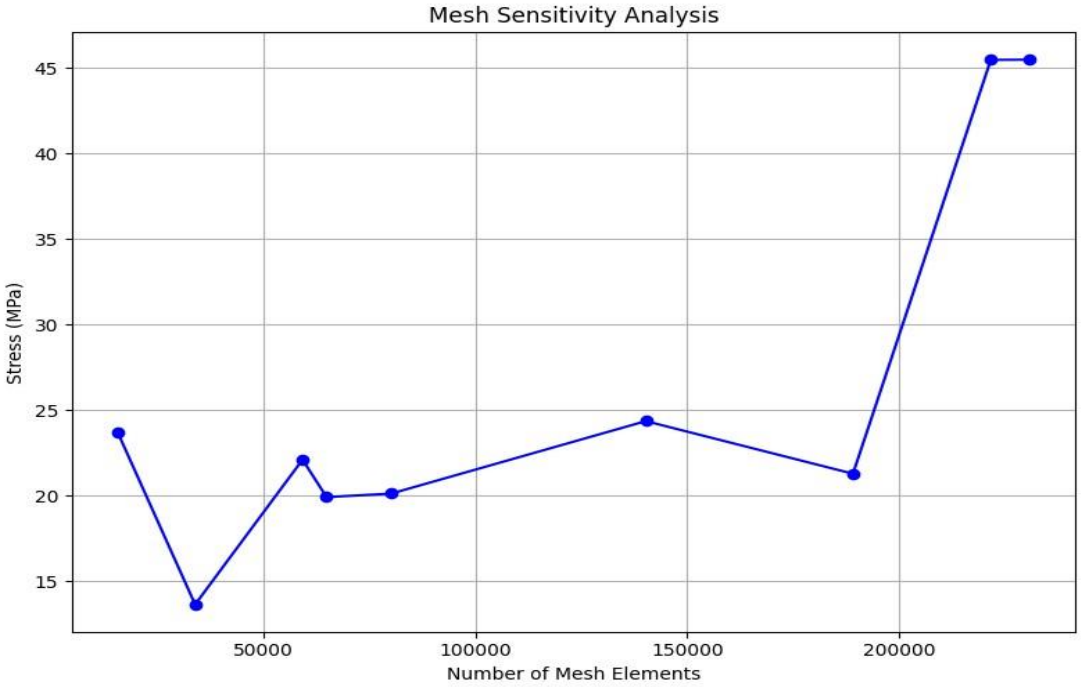

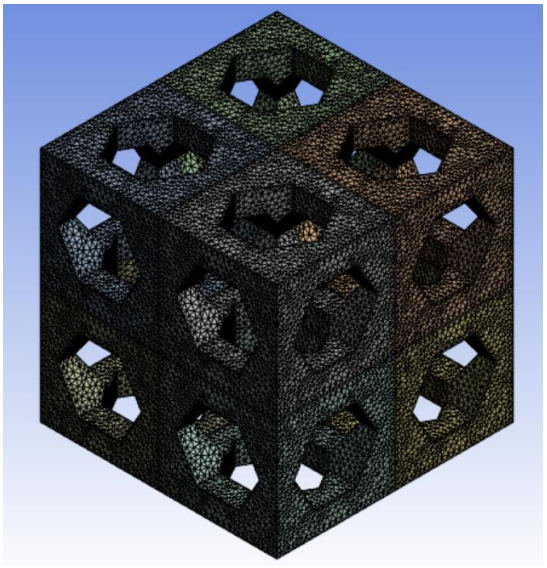

Figure **3-4**: Mesh sensitivity analysis of a hollow hexagon model (HH2) when subjected to a displacement load 10% of its total height and mesh model of HH2.

Boundary Conditions

1. Hollow Circular Geometry Structures:

- The models are compressed with a displacement equivalent to 5% of their total height.
- The bottom part of each model is fixed, as illustrated in Figure 3-5.
- The simulation time period is set to 1 second, with an increment of 0.01 seconds, to capture the detailed response of the structures under the applied loads.

2. Hollow Cube and Truncated Hexahedron Models:

- These models are subjected to a load of 10N.
- The bottom part of each model is fixed, as illustrated in Figure 3-5.
- The simulation time period is set to 1 second, to capture the detailed response of the structures under the applied loads.

3. Hollow Hexagon, Truncated Cube and Hollow Elliptical Structures:

- These models undergo a displacement load of 5% of its total height,
- The bottom part of each model is fixed, as illustrated in Figure 3-5.
- The simulation time period is set to 1 second, to capture the detailed response of the structures under the applied loads.

Static loading is preferred in scaffold simulations due to its ability to mimic steady-state conditions and provides a better understanding of material behavior under constant loading of normal physiological stresses. The time dependence of loading in these simulations shows a nonlinear response, which is important for accurate prediction of scaffold performance.

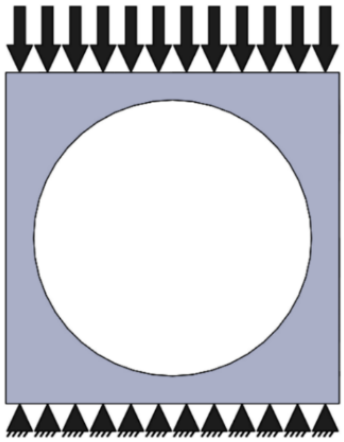

Figure **3-5**: Boundary condition of the model [40].

Validation of benchmark models

Hollow Cube and Truncated Hexahedron

During the evaluation of the hollow cube and truncated hexahedral structures, the results showed an unexpected phenomenon: the stress increases with decreasing porosity, which contradicts the general behaviour of decreasing porosity for higher tensile strength. Due to the inconsistencies, the results for the hollow cube and truncated hexahedral structures were excluded from further analysis.

Instead, the emphasis will remain on the hollow circle, which exhibits consistent and expected behaviour in relation to porosity and stress. Data and results for the hollow circle models are stored and highlighted to provide a more accurate representation of performance.

Hollow Circle

Figure 3-6 shows the finite element analysis (FEA) simulations of three scaffold models (labeled C1, C8, and C64) performed using ANSYS software. Each model has a uniform porosity of 81%, and voids account for 81% of the total volume. The overall dimensions of the models are 12x12x12 mm, with each unit cell adjusted to fit the dimensions. The main difference between these models is their total surface area.

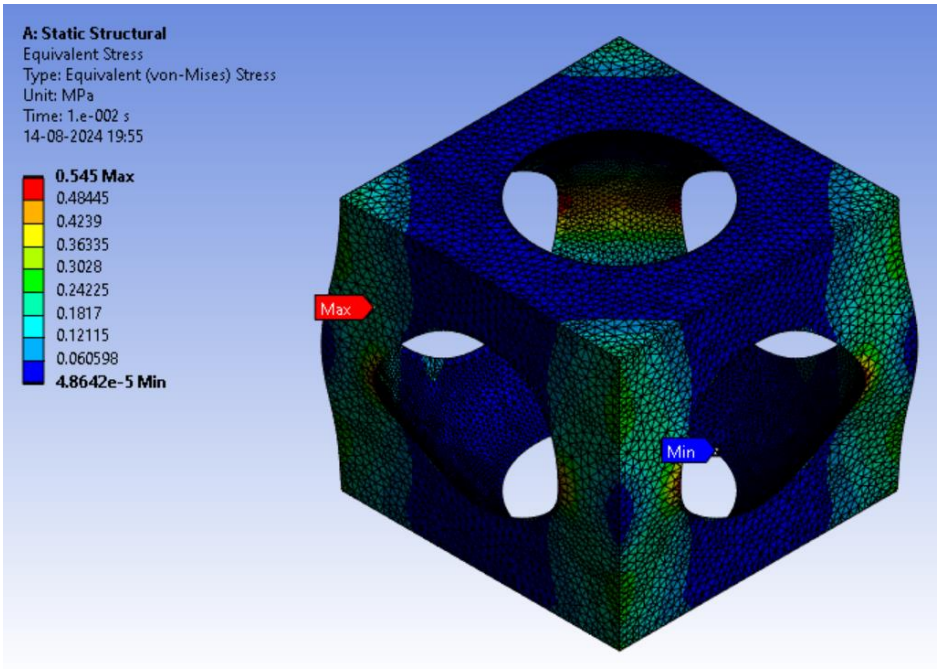

(a)

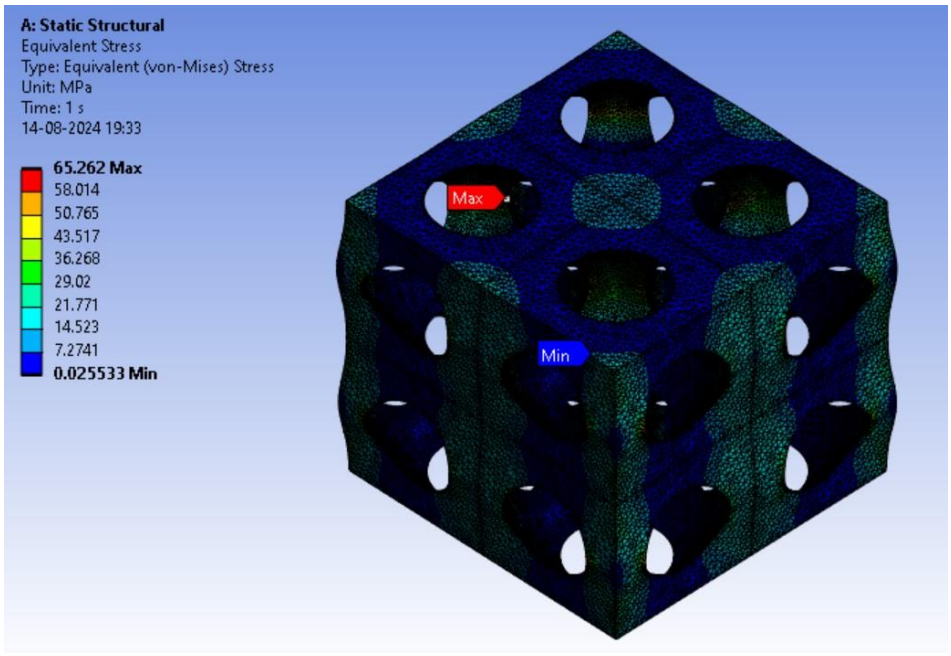

(b)

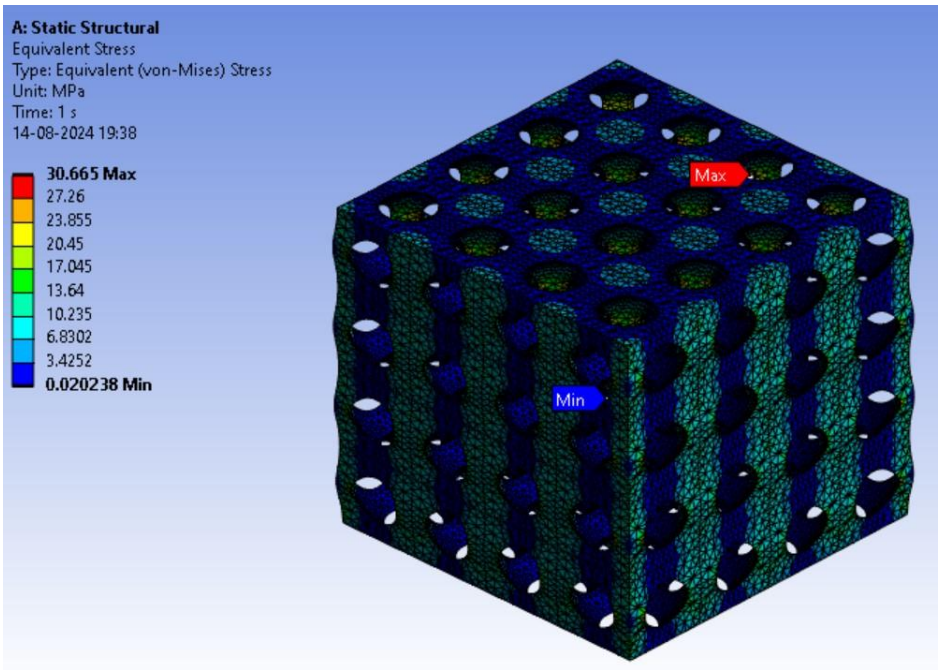

(c)

Figure **3-6**: Von Mises distribution of (a) C1, (b) C8 and (c) C64 at an early time step.

Analysis of the data in Table 3-2 and Figure 3-6 demonstrates the relationship between greater surface area, increased contact points, and greater resistance to compressive force, which increases safety. This is further supported by the stress-strain curves shown in Figure 3-7, which compares the performance of C1, C8, and C64 under stress. These findings are consistent with the work of Noordin et al. [40] who also reported that scaffold surface area construction can increase compression resistance. This recognition highlights the important role of surface optimization in improving scaffold performance for tissue engineering and regenerative medicine.

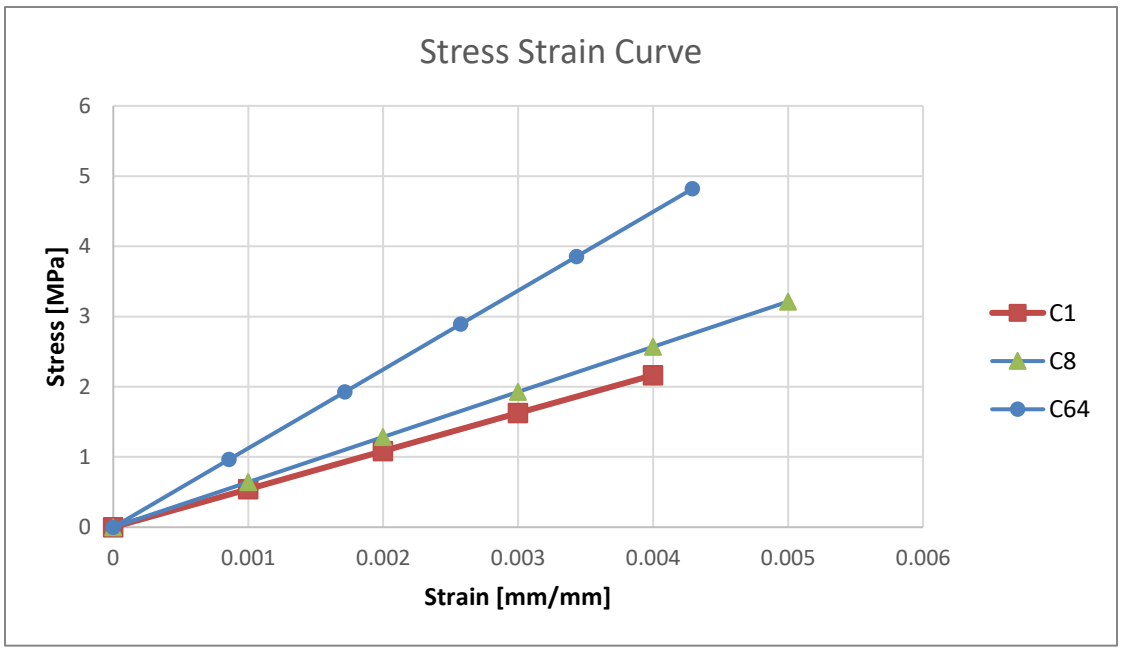

Figure **3-7**: Stress strain curve of C1, C8 and C64 under 5% displacement at an early time step.

Summary of validation of benchmark models

FEA simulations of the C1, C8, and C64 scaffold models confirm the accuracy of the simulation method used in this study. The C1, C8, and C64 models maintain consistent porosity by adjusting cell size to match the overall dimensions, allowing for a comparative analysis of different

scaffold configurations. The results illustrate how changes in cell size affect compressive stress distribution and overall stability.

The high consistency between the simulation results and the model results demonstrates the reliability of the model and provides a solid basis for further evaluation of the new model. The hollow cube and truncated hexahedron results were removed due to inconsistency with the observed and expected behavior in the stress response for different porosities.

Chapter 4

Results

Hollow Hexagon

In this study, hollow hexagonal structures using grade 5 titanium alloy were analysed using nonlinear simulations because the von Mises stress in the linear analysis exceeds the ultimate tensile strength of the material. This study investigates how the difference in porosity affects the compressive capacity and stress of the samples. The following properties of grade 5 titanium alloy were used in the simulations: Young's modulus of 110 GPa, Poisson's ratio 0.3, tensile yield strength 1098 MPa, ultimate tensile strength 1237 MPa, compressive yield strength 960 MPa, ultimate tensile strength. for 1098 MPa [43].

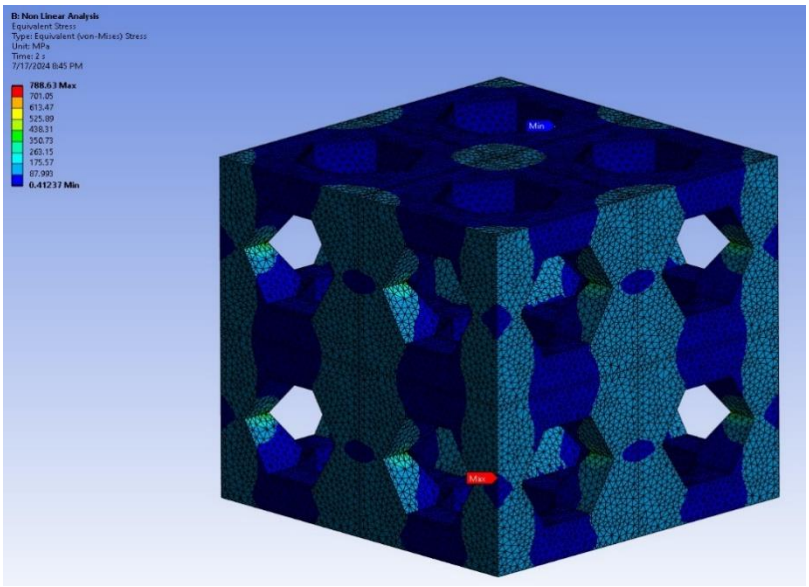

(a)

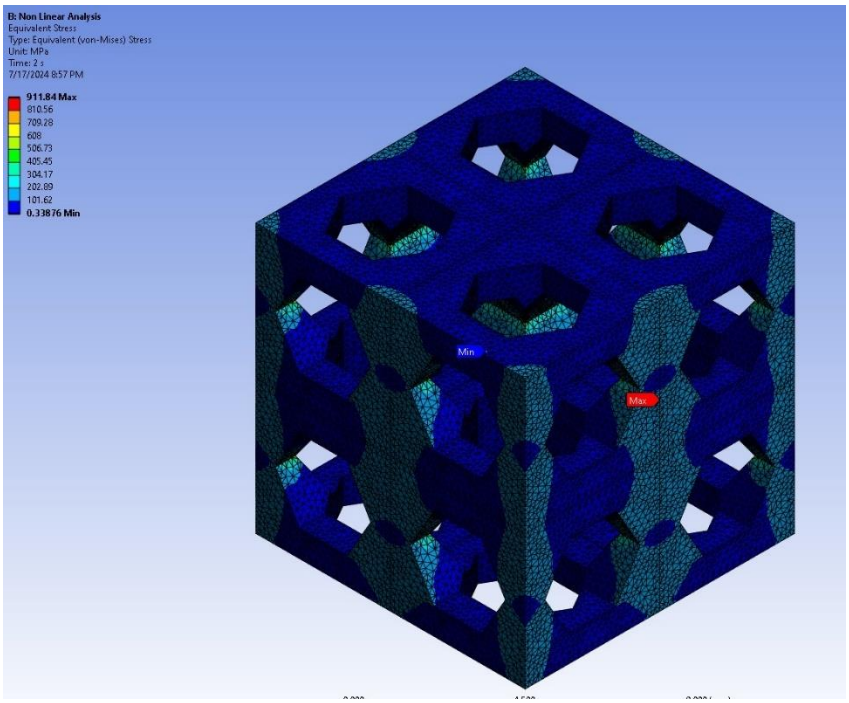
B: Non Linear Analysis
Equivalent Stress
Type: Equivalent (von-Mises) Stress
Unit: MPa
Time: 2 s
7/17/2024 8:57 PM
911.84 Max
810.56
709.28
608
506.73
405.45
304.17
202.89
101.62
0.33876 Min
Min
Max

(b)

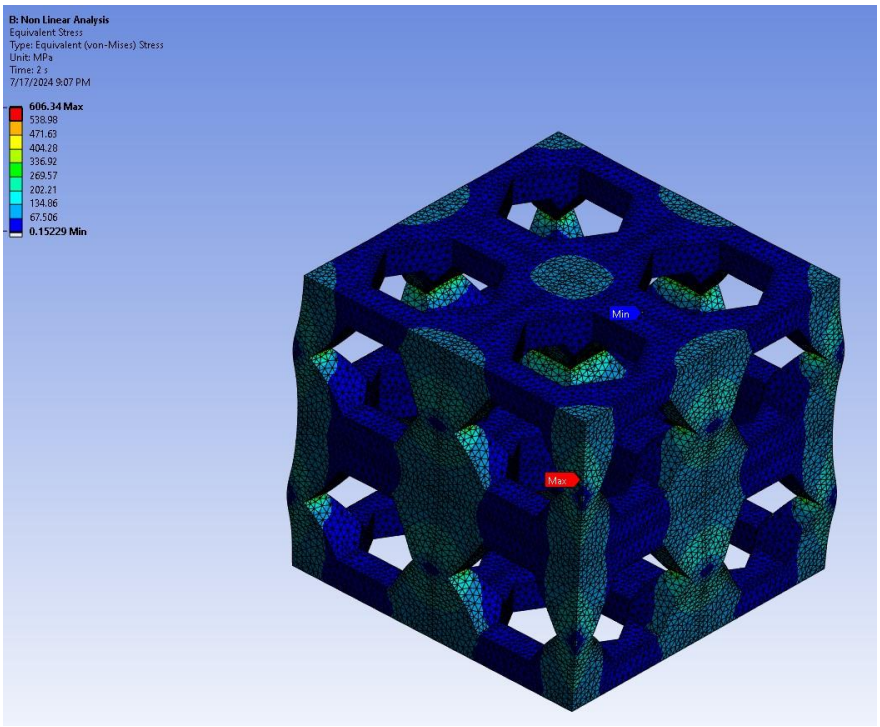
B: Non Linear Analysis
Equivalent Stress
Type: Equivalent (von-Mises) Stress
Unit: MPa
Time: 2 s
7/17/2024 9:07 PM
606.34 Max
538.98
471.63
404.28
336.92
269.57
202.21
134.86
67.506
0.15229 Min
Min
Max

(c)

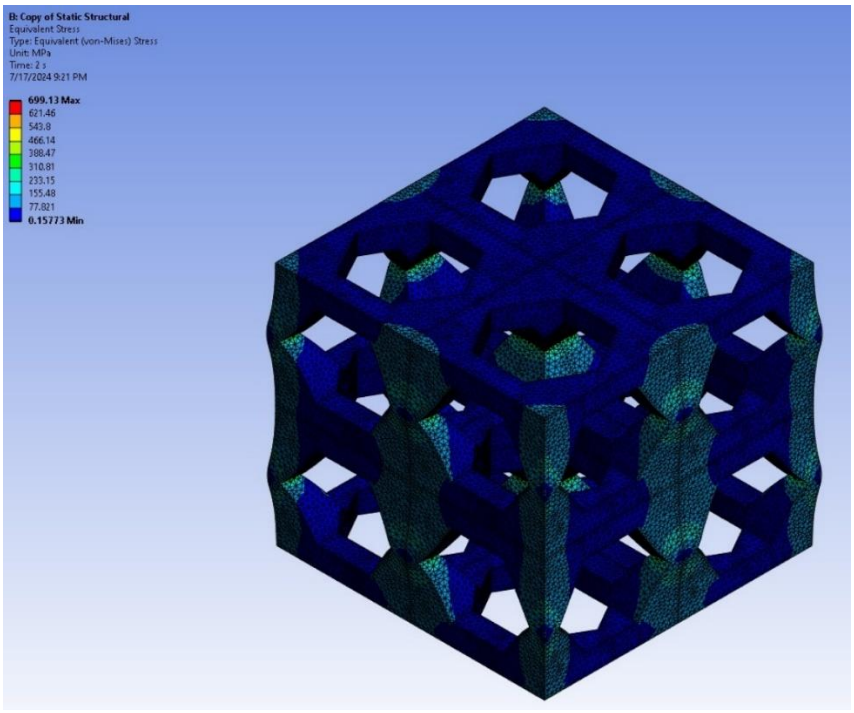

(d)

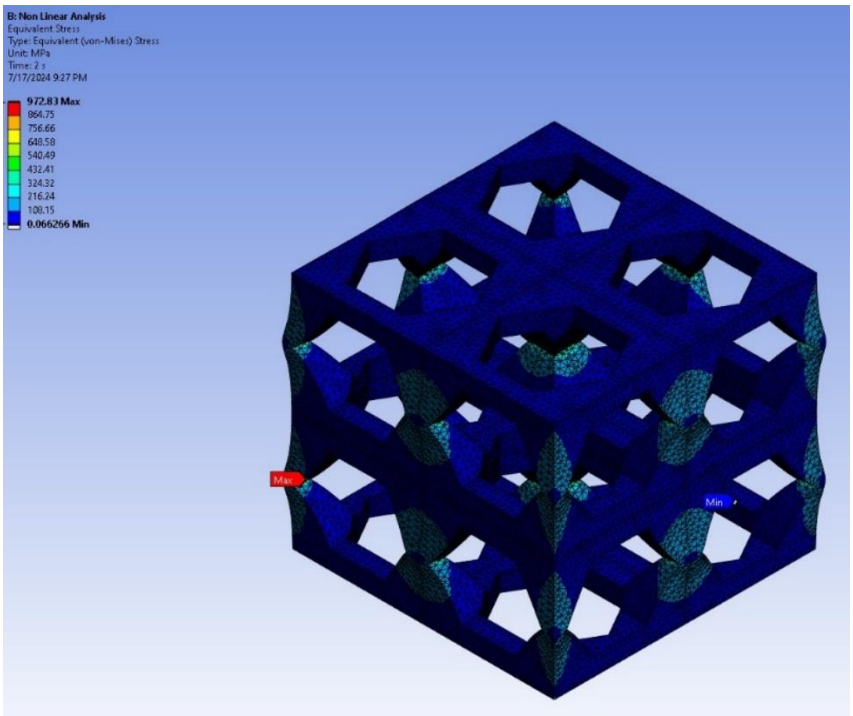

(e)

Figure **4-1**: Von Mises distribution of hollow hexagonal models with

(a) 50% porosity (HH1)
(b) 60% porosity (HH2)
(c) 70% porosity (HH3)
(d) 80% porosity (HH4)
(e) 90% porosity (HH5).

From Figure 4-1 and Table 3-3, it can be seen that increasing the porosity of the hollow hexagonal structure can increase the compressive capacity. This demonstrates the effectiveness of the stress distribution in the hexagonal framework, which is important for maintaining structural integrity as a load-bearing material.

Key findings for the hollow hexagon models include:

1. **Increased Compressive Load Capacity:** Higher porosity levels result in enhanced ability to withstand compressive loads, leveraging the high strength properties of titanium alloy grade 5.

2. **Surface Area and Mechanical Stability:** Although the surface area may decrease as porosity increases, the models exhibit high load-carrying capacity, demonstrating the balance of porosity and mechanical stability achieved with Grade 5 titanium alloys.

3. **Effective Stress Distribution:** The hollow hexagon design effectively distributes stress throughout its framework, reducing local failures and making the overall structure stronger under compression.

These findings indicate that hollow hexagonal structures using grade 5 titanium alloy have a good balance between high porosity, strong compressive load capacity, and reliable stress

resistance. The integrity of this structure indicates its suitability for applications requiring durability and porosity control, especially in the biomedical field, such as bone scaffolds.

The graph in Figure 4-2 shows the maximum compressive strength achieved by each model.

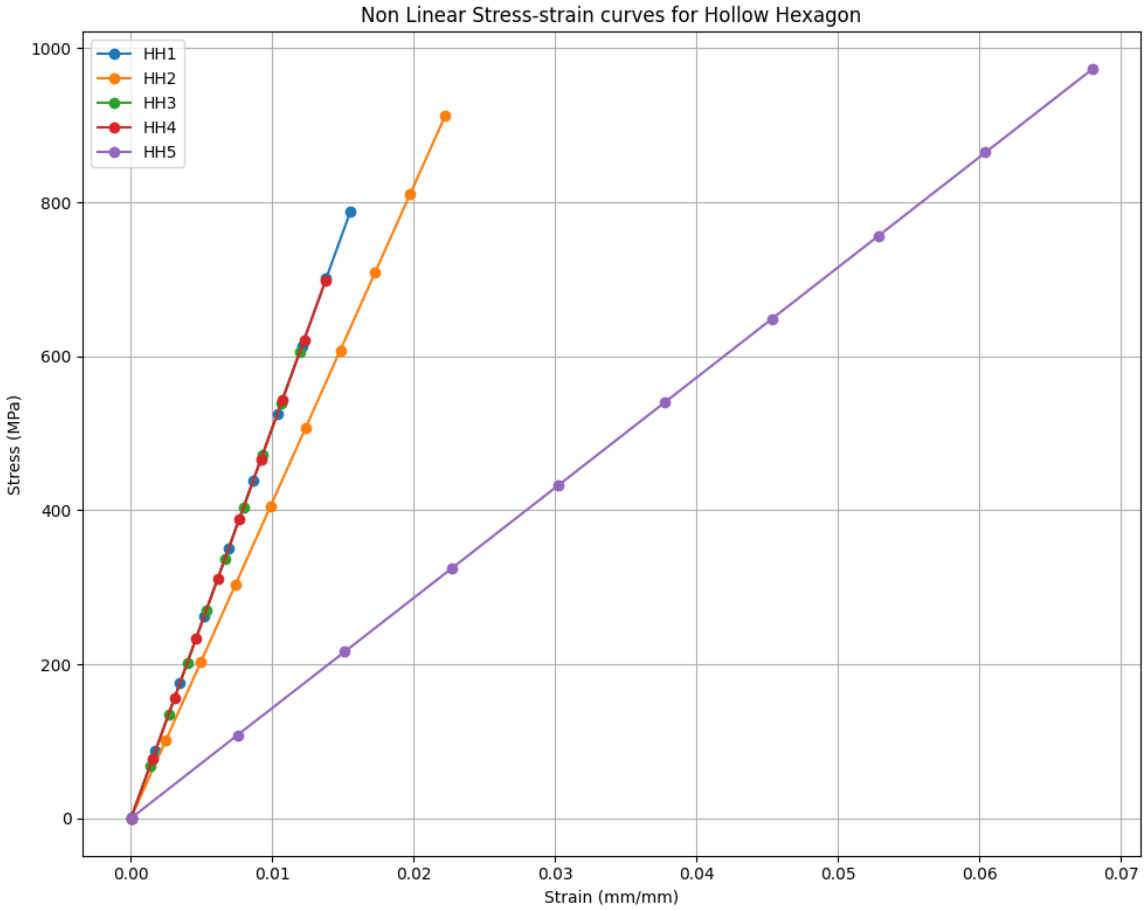

Figure **4-2**: Maximum compressive strength attained by each hollow hexagon model. HH1, HH2, HH3, HH4, and HH5 represent models with porosities of 50%, 60%, 70%, 80%, and 90%, respectively.

Truncated Cube

In this study, the truncated cubic model using the same material (grade 5 titanium alloy) as the hollow hexagon was evaluated to check the compressive load capacity and stress distribution at different porosity levels. As with the hollow hexagon, nonlinear simulations are used because the von Mises stress exceeds the ultimate tensile strength of the material in a linear analysis. This study aims to understand how the change in porosity affects the performance of the truncated cubic structure.

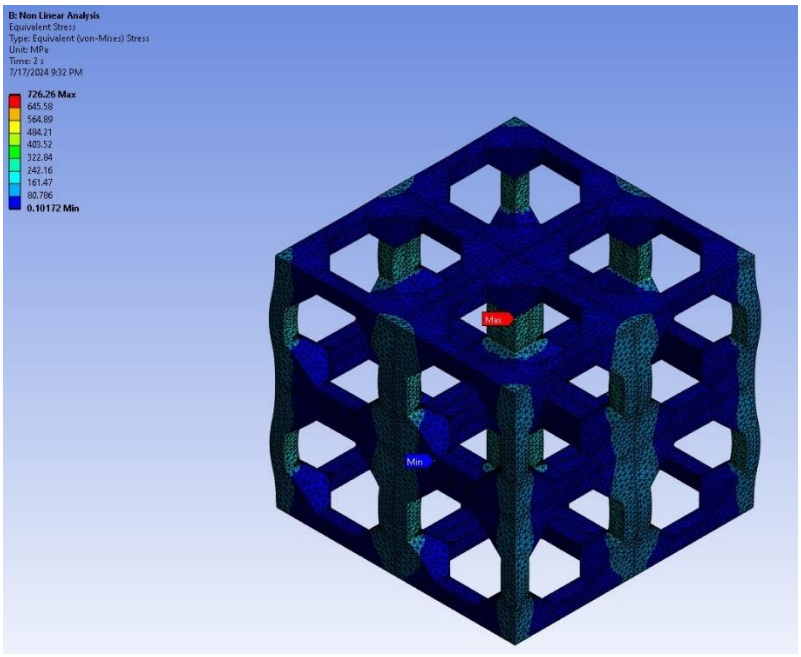

(a)

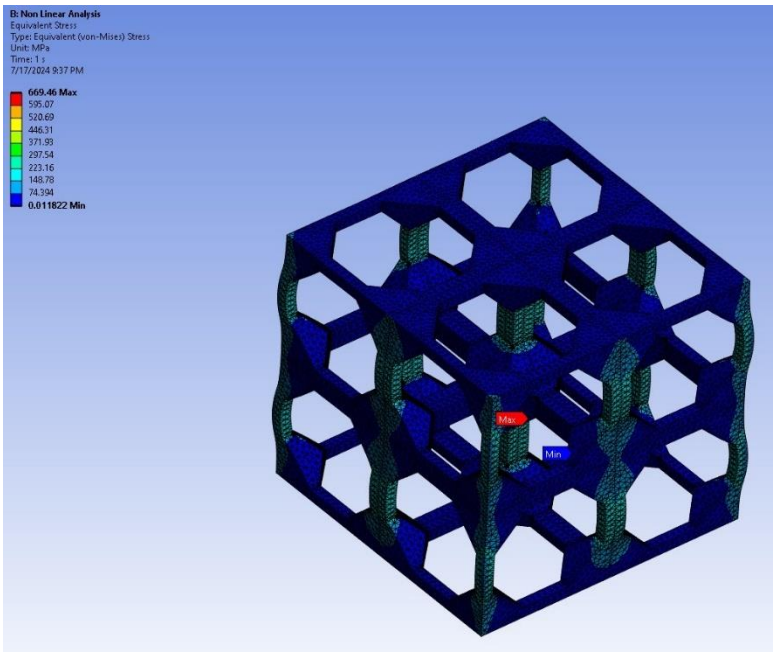
B: Non Linear Analysis
Equivalent Stress
Type: Equivalent (von-Mises) Stress
Unit: MPa
Time: 1 s
7/17/2024 9:37 PM
669.46 Max
595.07
520.69
446.31
371.93
297.54
223.16
148.78
74.394
0.011822 Min
Max
Min

(b)

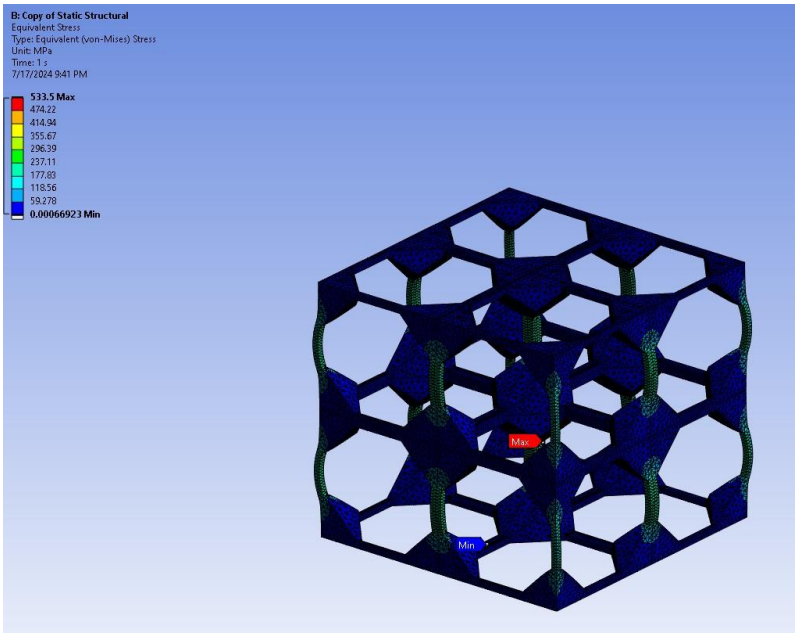
B: Copy of Static Structural
Equivalent Stress
Type: Equivalent (von-Mises) Stress
Unit: MPa
Time: 1 s
7/17/2024 9:41 PM
533.5 Max
474.22
414.94
355.67
296.39
237.11
177.83
118.56
59.278
0.00066923 Min
Max
Min

(c)

Figure **4-3**: Von Mises distribution of truncated cube models with
(a) 50% porosity (TRC1)
(b) 60% porosity (TRC2)
(c) 70% porosity (TRC3)

From Figure 4-3 and Table 3-4, it is observed that the maximum load capacity decreases as the porosity of the truncated cubic specimen using grade 5 titanium alloy increases. This indicates that there is a balance between porosity and load carrying capacity in the truncated cube design. The maximum porosity is 70% due to the small geometry of the truncated cube, as higher porosity will affect the structural integrity considering the selected length.

Key findings for the truncated cube models include:

1. **Decreased Compressive Load Capacity:** The data show the relationship between porosity and the ability of the structure to withstand loads. An increase in porosity reduces the load capacity, indicating a decrease in the structural integrity of the truncated cube design.

2. **Surface Area and Mechanical Stability:** Higher porosity not only reduces the load capacity but also affects mechanical stability. The results show that although some are stable, increased porosity affects overall strength, which is important for applications requiring a strong load capacity.

3. **Stress Distribution:** As porosity increases, the truncated cube creates uneven stress, resulting in higher stress and points of failure. This indicates the need to optimize the balance of porosity and structural integrity.

4. **Comparison with Hollow Hexagon:** Compared to the hollow hexagonal structure using Grade 5 titanium alloy, the truncated cubes show that although the material is strong, its geometric design greatly affects the load-carrying capacity. The decrease in efficiency at higher porosity highlights the important role of material selection and geometry in scaffold design.

These findings confirm the hypothesis that increasing porosity in the truncated cubic structure leads to a decrease in maximum compressive load capacity. The observed decrease in load capacity with increasing porosity, together with the inequality of stress, highlights the need to optimize cube design in applications where porosity and strength are crucial.

The graph in Figure 4-4 shows the maximum compressive strength achieved for each truncated cube specimen as the porosity level increases.

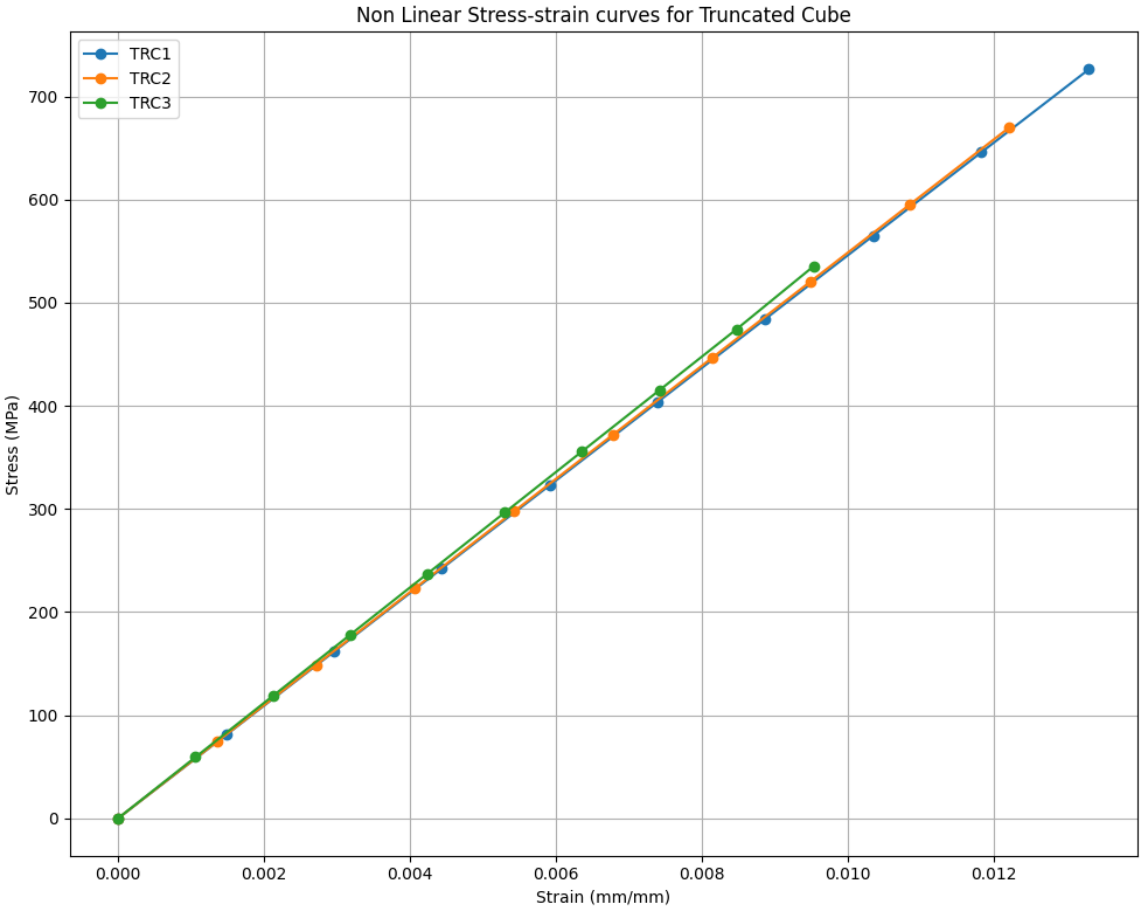

Figure **4-4**: Maximum compressive strength attained by each truncated cube model. TRC1, TRC2, and TRC3, represent models with porosities of 50%, 60%, and 70%, respectively .

Hollow Elliptical

In this study, hollow elliptical scaffold made of grade 5 titanium alloy, similar to hollow hexagonal and truncated cube models, was evaluated using linear analysis. This study investigates the load capacity and stress in a variable porosity model consisting of larger and smaller elliptical cells with a total porosity of approximately 26%. The analysis aims to understand how changes in

porosity level affect the performance of hollow elliptical scaffolds which did not exceed the ultimate tensile strength of the material.

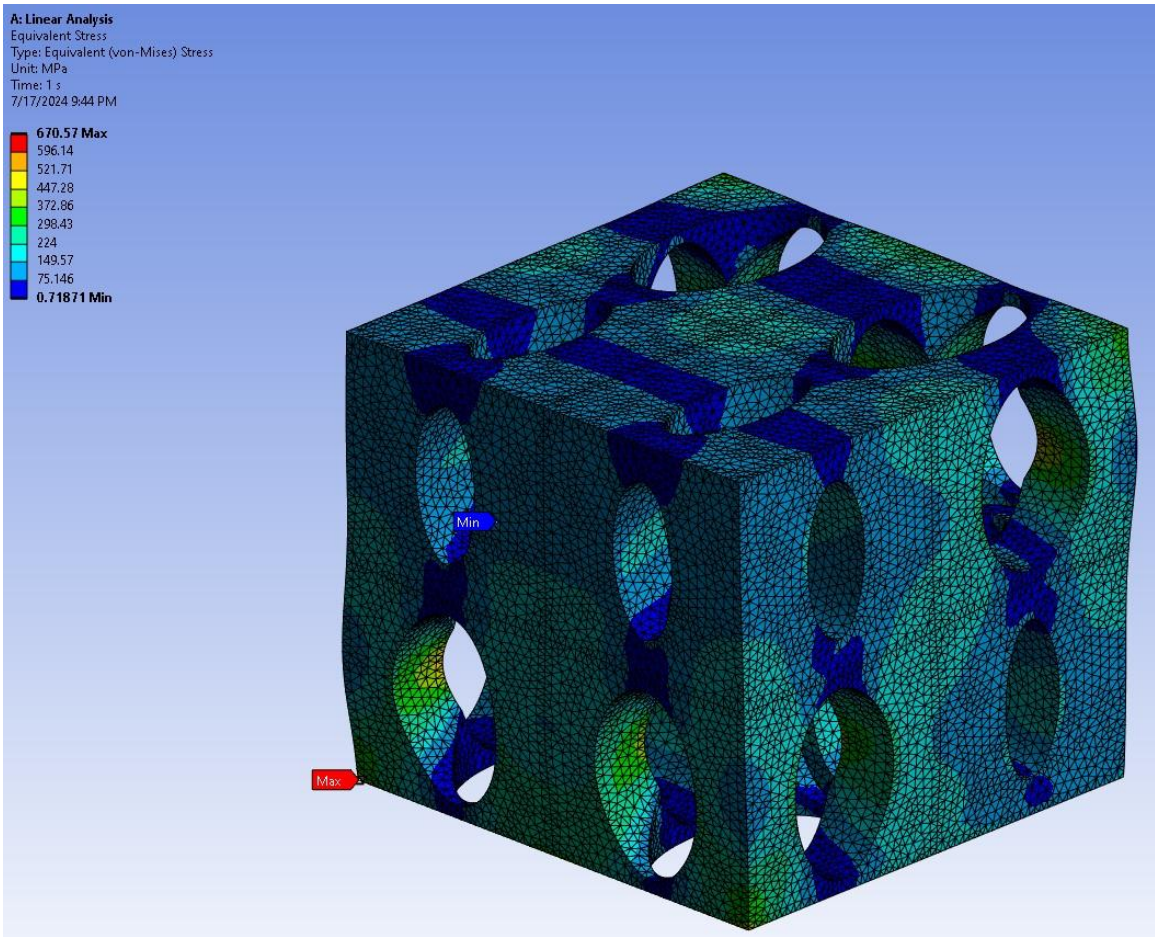

Figure **4-5**: Von Mises stress distribution in the Hollow Elliptical Scaffold .

Due to its low porosity, the hollow elliptical scaffold did not require a nonlinear analysis. The results showed that the scaffold exhibited slightly lower compressive load capacity compared to the truncated cube and hollow hexagonal structures. This is illustrated by the von Mises stress distribution in the hollow elliptical scaffold shown in Figure 4-5 and the maximum compressive strength attained by the scaffold presented in Figure 4-6. This indicates that when the hollow

elliptical scaffold uses grade 5 titanium alloy, its performance in compression loading is slightly lower than the truncated cube and hollow hexagonal designs.

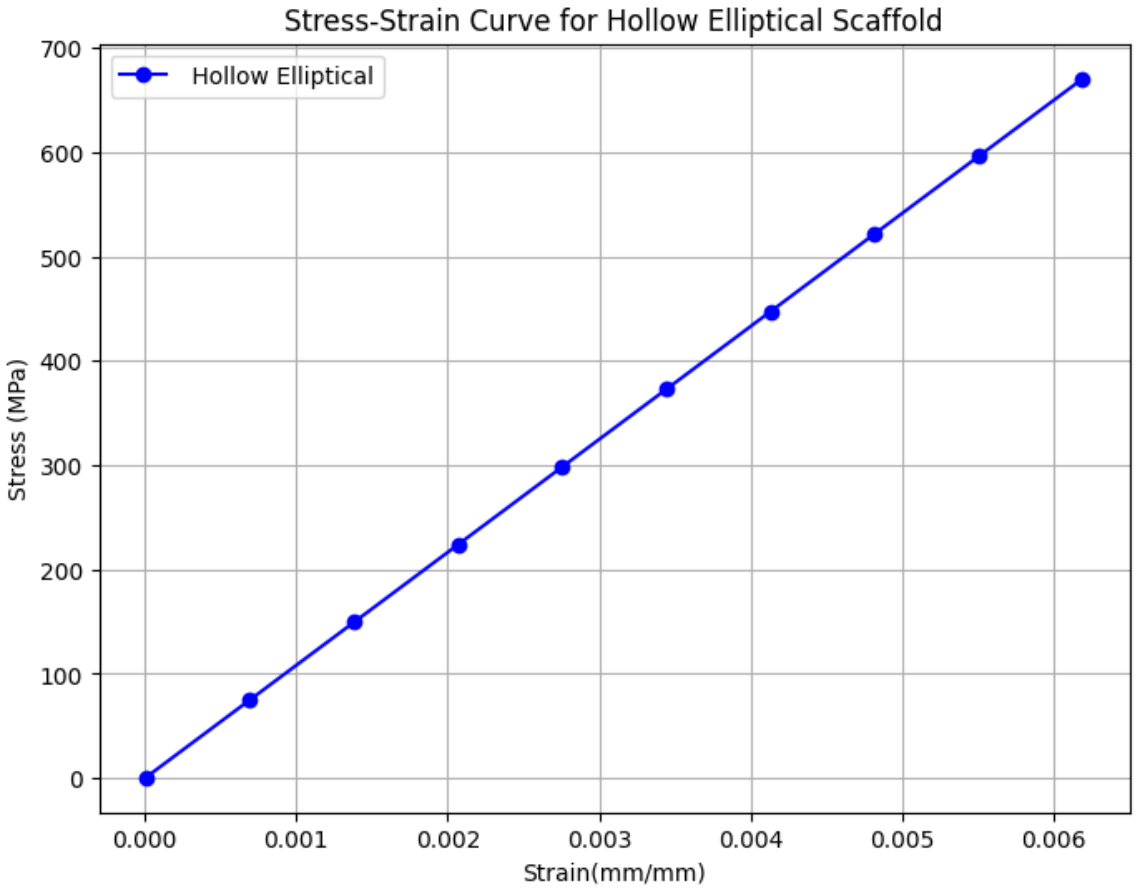

Figure **4-6**: Maximum compressive strength attained by the hollow elliptical scaffold .

Chapter 5

Conclusion

This study evaluated the performance of hollow hexagon, truncated cube, and hollow elliptical scaffold designs using finite element analysis to optimize structures for bone regeneration. Key findings include:

- **Hollow Hexagon:** Increased porosity resulted in increased compressive load capacity, however, it was accompanied by a decrease in overall surface area, which affected mechanical stability.

- **Truncated Cube:** As porosity increases, the maximum compressive load capacity decreased, indicating a balance between porosity and load-carrying capacity. The small geometry of the truncated cube limited the maximum porosity to 70%.

- **Hollow Elliptical:** This model performed well with varying porosity, reaching a total porosity of approximately 26%. Due to its low porosity, linear analysis was sufficient to not exceed the ultimate tensile strength of the material.

These findings highlight the need to optimize scaffold design to balance porosity, integrity, and overall stability. Thicker struts in the truncated cube increases stability in terms of compressive stress tolerance, while higher porosity in the hollow ellipse structure can improve stress distribution and overall ware. These insights may aid in the development of orthopedic materials and technologies designed to facilitate loading and biological performance in bone tissue engineering.

References

1. D.P. Emlyn Forsung, J.A. Cameron, Current concepts with autogenous bone grafting, Podiatry Today. 33 (7) (2020).
2. G.F. Rogers, A.K. Greene, Autogenous bone graft: basic science and clinical implications, J. Craniofacial Surg. 23(1) (2012) 323-7. (https://doi.org/10.1097/SCS.0b013e318241dcba).
3. P. Chocholata, V. Kulda, V. Babuska, Fabrication of scaffolds for bone-tissue regeneration, Materials 12 (2019).
4. X. Wang, S. Xu, S. Zhou, W. Xu, M. Leary, P. Choong, M. Qian, M. Brandt and Y. M. Xie, "Topological design and additive manufacturing of porous metal for bone scaffolds and orthopedicsimplants: A review," Biomaterials, vol. 83, pp. 127-141, 2016.
5. M. Leary, M. Mazur, J. Elambasseril, M. McMillan, T. Chirent, Y. Sun, M. Qian, M. Easton and M. Brandt,"Selective laser melting (SLM) of AlSi12Mg lattice structures," Materials and Design, vol. 98, pp. 344–357, 2016.
6. Q. Chen and G. A. Thouas, "Metallic implant biomaterials," Materials Science and Engineering R, vol. 87, pp. 1-57, 2015.
7. Y. F. Zheng, X. N. Gu and F. Witte, "Biodegradable metals," Materials Science and Engineering R, vol. 77, pp. 1-34, 2014.
8. Bhardwaj, Tarun & Singh, Surya & Shukla, Dr Mukul. (2017). Finite Element Modelling and Analysis of Implant Scaffolds. 10.1109/AMIAMS.2017.8069239.
9. Giannitelli SM, Accoto D, Trombetta M, Rainer A. Current trends in the design of scaffolds for computer-aided tissue engineering. Acta Biomater. 2014 Feb;10(2):580-94. doi: 10.1016/j.actbio.2013.10.024. Epub 2013 Oct 30. PMID: 24184176.

10. Tan KH, Chua CK, Leong KF, Cheah CM, Cheang P, Abu Bakar MS, Cha SW. Scaffold development using selective laser sintering of polyetheretherketone-hydroxyapatite biocomposite blends. Biomaterials. 2003 Aug;24(18):3115-23. doi: 10.1016/s0142-9612(03)00131-5. PMID: 12895584.
11. W. Sun, B. Starly, J. Nam, A. Darling,Bio-CAD modeling and its applications in computer-aided tissue engineering,Computer-Aided Design,Volume 37, Issue 11,2005.
12. Echeverria Molina Maria I., Malollari Katerina G., Komvopoulos Kyriakos (2021), Design Challenges in Polymeric Scaffolds for Tissue Engineering, Frontiers in Bioengineering and Biotechnology, Volume 9.
13. Moreno Madrid, A.P.; Vrech, S.M.; Sanchez, M.A.; Rodriguez, A.P. Advances in additive manufacturing for bone tissue engineering scaffolds. *Materials Science and Engineering: C* **2019**, *100*, 631-644, doi:https://doi.org/10.1016/j.msec.2019.03.037.
14. Kazimierczak, P.; Benko, A.; Nocun, M.; Przekora, A. Novel chitosan/agarose/hydroxyapatite nanocomposite scaffold for bone tissue engineering applications: comprehensive evaluation of biocompatibility and osteoinductivity with the use of osteoblasts and mesenchymal stem cells. *International journal of nanomedicine* **2019**, *14*, 6615-6630, doi:https://doi.org/10.2147/IJN.S217245.
15. Carluccio, D.; Xu, C.; Venezuela, J.; Cao, Y.; Kent, D.; Bermingham, M.; Demir, A.G.; Previtali, B.; Ye, Q.; Dargusch, M. Additively manufactured iron-manganese for biodegradable porous load-bearing bone scaffold applications. *Acta Biomaterialia* **2020**, *103*, 346-360, doi:https://doi.org/10.1016/j.actbio.2019.12.018.
16. Chen, Z.; Yan, X.; Yin, S.; Liu, L.; Liu, X.; Zhao, G.; Ma, W.; Qi, W.; Ren, Z.; Liao, H., et al. Influence of the pore size and porosity of selective laser melted Ti6Al4V ELI porous scaffold on cell proliferation, osteogenesis and bone ingrowth. *Materials Science and Engineering: C* **2020**, *106*, 110289, doi:https://doi.org/10.1016/j.msec.2019.110289.

17. Ngadiman, N.H.A.; Noordin, M.Y.; Idris, A.; Kurniawan, D. A review of evolution of electrospun tissue engineering scaffold: From two dimensions to three dimensions. *Proceedings of the Institution of Mechanical Engineers, Part H: Journal of Engineering in Medicine* **2017**, *231*, 597-616, doi:https://doi.org/10.1177/0954411917699021.
18. Chocholata, P.; Kulda, V.; Babuska, V. Fabrication of scaffolds for bone-tissue regeneration. Materials **2019**, 12, 568.
19. Kumar A, Jacob A. Techniques in scaffold fabrication process for tissue engineering applications: A review. J Appl Biol Biotech. 2022; 10(03):163–176.
20. Pan, C.; Han, Y.; Lu, J. Design and Optimization of Lattice Structures: A Review. Appl. Sci. **2020**, 10, 6374.
21. H. Gong, et al., Analysis of defect generation in Ti-6Al-4V parts made using powder bed fusion additive manufacturing processes, Addit. Manuf. 1 (2014) 87e98.
22. A.A. Zadpoor, Mechanical performance of additively manufactured meta biomaterials, Acta Biomater. (2018).
23. Edgar B. Montufar, Serhii Tkachenko, Mariano Casas-Luna, Pavel Škarvada, Karel Slámečka, Sebastian Diaz-de-la-Torre, Daniel Koutný, David Paloušek, Zuzana Koledova, Laura Hernández-Tapia, Tomáš Zikmund, Ladislav Čelko, Jozef Kaiser, Benchmarking of additive manufacturing technologies for commercially-pure-titanium bone-tissue engineering scaffolds: processing-microstructure-property relationship, Additive Manufacturing, Volume 36,2020
24. Ran Q, Yang W, Hu Y, She X, Yu Y, Xiang Y, Cai K. Osteogenesis of 3D printed porous Ti6Al4V implants with different pore sizes. J Mech Behav Biomed Mater. 2018;84:1–11.

25. Ouyang P, Dong H, He X, Cai X, Wang Y, Li J, Li H, Jin Z. Hydromechanical mechanism behind the effect of pore size of porous titanium scaffolds on osteoblast response and bone ingrowth. Mater Des. 2019;183.

26. Taniguchi N, Fujibayashi S, Takemoto M, Sasaki K, Otsuki B, Nakamura T, Matsushita T, Kokubo T, Matsuda S. Effect of pore size on bone ingrowth into porous titanium implants fabricated by additive manufacturing: an in vivo experiment. Mat Sci Engineering C-Materials for Biological Applications. 2016;59:690–701.

27. Otsuki B, Takemoto M, Fujibayashi S, Neo M, Kokubo T, Nakamura T. Pore throat size and connectivity determine bone and tissue ingrowth into porous implants: three-dimensional micro-CT based structural analyses of porous bioactive titanium implants. Biomaterials. 2006;27(35):5892–900.

28. Karageorgiou V, Kaplan D. Porosity of 3D biomaterial scaffolds and osteogenesis. Biomaterials. 2005;26(27):5474–91.

29. Kadkhodapour, J.; Montazerian, H.; Darabi, A.C.; Anaraki, A.P.; Ahmadi, S.M.; Zadpoor, A.A.; Schmauder, S. Failure mechanisms of additively manufactured porous biomaterials: Effects of porosity and type of unit cell. J. Mech. Behav. Biomed. Mater. **2015**, 50, 180–191.

30. Z.U. Arif, M.Y. Khalid, A. Zolfagharian, M. Bodaghi, 4D bioprinting of smart polymers for biomedical applications: recent progress, challenges, and future perspectives. React. Funct. Polym. (2022) 105374. (https://doi.org/10.1016/j.reactfunctpolym.2022.105374).

31. S.L. Sing, Y. Miao, F.E. Wiria, W.Y. Yeong, Manufacturability and mechanicaltesting considerations of metallic scaffolds fabricated using selective lasermelting: a review, Biomed. Sci. Eng. 1 (1) (2016).

32. H. Hasib, O.L.A. Harrysson, H.A. West, Powder removal from Ti-6Al-4 V cellularstructures fabricated via electron beam melting, JOM 67 (3) (2015) 639–646.

33. Yang, You-wen et al. “Additive manufacturing of bone scaffolds.” *International Journal of Bioprinting* 5 (2018): n. pa

34. J.J. Bara, F. Guilak, Engineering functional tissues: in vitro culture parameters, Princ. Tissue Eng. (2020) 157-177. Academic Press. https://doi.org/10.1016/ B978-0-12-818422-6.00011-3.

35. S. Bose, M. Roy, A. Bandyopadhyay, Recent advances in bone tissue engineering scaffolds. Trends Biotechnol. 30(10) (2012) 546-54. https://doi.org/10.1016/j.tibtech.2012.07.005.

36. Smith, M.; Guan, Z.; Cantwell, W.J. Finite element modelling of the compressive response of lattice structures manufactured using the selective laser melting technique. Int. J. Mech. Sci. **2013**, 67, 28–41.

37. Frich LH, Jensen NC, Odgaard A, Pedersen CM, Søjbjerg JO, Dalstra M. Bone strength and material properties of the glenoid. J Shoulder Elbow Surg. 1997 Mar-Apr;6(2):97-104. doi: 10.1016/s1058-2746(97)90029-x. PMID: 9144596.

38. Lei, Jianyin & Dong, Pengfei & Li, Zhiqiang & Zhu, Feng & Wang, Zhihua & Cai, Xianhua. (2017). Biomechanical analysis of the fixation systems for anterior column and posterior hemi-transverse acetabular fractures. Acta Orthopaedica et Traumatologica Turcica. 51. 10.1016/j.aott.2017.02.003.

39. Kaushlendra Kumar, Ram Bilas Prasad, Stress analysis of cortical bone of human femur, Materials Today: Proceedings, Volume 44, Part 1, 2021, Pages 2054-2060, ISSN 2214-7853, https://doi.org/10.1016/j.matpr.2020.12.166.

40. Noordin, Muhammad & Putra, Amir & Ngadiman, N.H.A. & Mustafa, Nur Syahirah & Mohd Yusof, Noordin & Ma'aram, Azanizawati. (2021). Finite Element Analysis of Porosity Effects on Mechanical Properties for Tissue Engineering Scaffold. Biointerface Research in Applied Chemistry. 11. 8836-8843. 10.33263/BRIAC112.88368843.
41. T. Bhardwaj, S. P. Singh and M. Shukla, "Finite element modeling and analysis of implant scaffolds," 2017 International Conference on Advances in Mechanical, Industrial, Automation and Management Systems (AMIAMS), Allahabad, India, 2017, pp. 358-362, doi: 10.1109/AMIAMS.2017.8069239.
42. N. E. Dowling, *Mechanical Behavior of Materials: Engineering Methods for Deformation, Fracture, and Fatigue*, 3rd ed. Pearson Education, 2006.
43. Zaharin HA, Abdul Rani AM, Azam FI, Ginta TL, Sallih N, Ahmad A, Yunus NA, Zulkifli TZA. Effect of Unit Cell Type and Pore Size on Porosity and Mechanical Behavior of Additively Manufactured Ti6Al4V Scaffolds. Materials (Basel). 2018 Nov 28;11(12):2402. doi: 10.3390/ma11122402. PMID: 30487419; PMCID: PMC6317238.